Imaging Process Overview and Design of an Unobscured Telescope

by

David Alejandro Villegas López

A Masters's Report Submitted to

James C. Wyant College of Optical Sciences

In Partial Fulfillment of the Requirements

For the Degree of

MASTER OF SCIENCE

In the Graduate College

THE UNIVERSITY OF ARIZONA

2021

Acknowledgments

There are no self-made men. Nobody can do it alone. For this reason, the list of people to thank is huge:

I would like to start with all those people who sowed the seed of the curiosity in my mind. They opened a window. My teachers at School, my Professors at University and my Mentors in the industry.

I would like to express my acknowledgments to my employers, for the time, the resources, and their understanding, especially at the end of the courses.

I would like to thank my mother who has invested her youth in my education. The first example of how to do a task till the end. Even in these three years of hard battle with the illness always willing to listen.

Finally, I would like to say thank you so much to Angélique, my rock, my safe place, my partner who is always ready to help with big and small things, day after day.

Table of Contents

Abstract

This report provides and overview of the study of imaging in Master course. The report has to main parts: The first one cover the theoretical part the imaging process from geometric optics till aberration theory. In this part of the report a quick review of concepts as: collinear transformations, Gaussian equations, symmetry in optical systems, Fourier optics and optical aberrations till sixth order aberration are reviewed. The second part is a practical case. Starting form an on-axis Cassegrain telescope, the process of design of an unobscured telescope based in extended polynomial surface is described, including the correction of all the aberration in the system till fourth order.

Abbreviations and symbols

‘ : Related to the image or image space
c: Wave speed propagation in the vacuum
F: Front focal point
F’: Rear focal point
HW: Homework
$\vec{\mathcal{H}}$: Magnetic field $\left(\mathcal{H}_x, \mathcal{H}_y, \mathcal{H}_z\right)$
m: Transverse magnification
n: Refraction index
OA: Optical Axis
OAR: Optical Axis Ray
P(x,y,z) : Point at (x,y,z)
P: Front principal plane
P’: Rear principal plane
P_w: General pupil function
P_{mn}: Polynomial in the form $x^m y^n$
$\overline{S}$: Stop Shifting Parameter
TTC: Tilted Component Telescope
$\vec{\mathcal{E}}$: Electric field $\left(\mathcal{E}_x, \mathcal{E}_y, \mathcal{E}_z\right)$
μ: Magnetic permeability of the medium
ϵ: Electric permittivity medium
ϵ_0: Vacuum permittivity
ρ: Normalized aperture vector
μ: Magnetic permeability of the medium
μ_0: Vacuum permeability
λ: Wavelength
v: Optical frequency
∇: Nabla operator $=\frac{\partial}{\partial x}\hat{x} + \frac{\partial}{\partial y}\hat{y} + \frac{\partial}{\partial z}\hat{z}$

List of Figures

1 Introduction

After two and a half years it is time to write this report, that allows me to recapitulate all that has happened during this academic challenge. I can divide the profit of the Master in 3 main aspects:

- New insights about known concepts. For example, the possibility of evaluation of aberrations using first order ray tracing.

- New perspectives. For example, the Fourier interpretation of optical systems and it similarities with other fields of Engineering through the transfer function and the theory of linear systems.

- New skills. For example, the development of a competency in using ray tracing software

This report deals with all these topics. Not too much in detail because there is material for several volumes, but in a way that it provides a consistent reference framework in key aspects of the Master, from the geometrical optics till the compensation of aberration in a plane symmetric system.

Chapter 2 introduces the general concept of linear transformation and the cases of axisymmetric and plane symmetry systems. For the first case the first order imaging equations with the coordinate system at the principal planes (Gaussian Equations) are deducted.

Chapter 3 deals with the wave nature of light, starting from Maxwell's equations, some concepts about diffraction theory including the equivalence between the propagation in free space based on the Point Spread Function (PSF) and the Fourier Transform approach.

In Chapter 4 the idea of the wavefront aberration at the pupil as phase shift function is presented. Then the wavefront aberration representation using power series expansion and the Seidel sums are introduced. This chapter also describes the effect of aspheric surfaces and the position of the stop in the wavefront aberration function. In the second section of chapter 3rd aberration of the axisymmetric are expanded to plane symmetric systems

Chapter 5 covers the practical part of the report focused on the design of a "Tilted Component Telescope" (TCT). The study plane symmetric systems is relevant for two reasons: First, it helps understanding what happens with axisymmetric systems when the elements are tilted by assembly and manufacturing tolerances. Second with the introduction of free form optics and the modern technology of manufacturing the design of unobscured system based in mirrors have gained more and more importance. Examples of this application are the modern systems of lithography using extreme ultraviolet (EUV) light for chips manufacturing. The practical part of the report is the design of a hypothetical TCT based on extended polynomial surfaces in OpticStudio. With a proper expansion and carefully selecting the polynomials to include in the surface it is possible to correct plane symmetric aberrations till the 4th order. Finally, and academic exercise about removing the remaining field curvature was carried out introducing a refractive element in the vicinity of the image plane. The design of this telescope is the outcome of an independent study performed under the tutorship of Professor Jose Sasián during the course of fall 2021.

2 Imaging systems

In the most general sense IMAGING is the process of formation of an image of a real object. The process involved always implies a transformation that can cover anything form the representation of a scene by a painter up to and including the image produced by a high-speed camera (time frequency) or high resolution camera (spatial frequency).

In the current document the process of image formation will be done by an optical system. That means that the light reflected or emitted by a three-dimensional object produces after passing through the system a three dimensional distribution of light. The space where the object exists is called *"object space"*, respectively, the space where the image exists is called the *"image space"*. Each space is infinite, and it has associated a refraction index. In a system with a number *n* of surfaces, each surface defines its own object and image space, in total a complete system has *n+1* optical spaces where the image of an element is the object of the next element.

Now, if from an ideal object point such that emitting rays in all directions, some of these rays pass through an image system, and if for each object point one and only one image point exists. A transformation between both spaces can be established and in the most general case its form is:

$$x' = x'(x,y,z) \quad y' = y'(x,y,z) \quad z' = z'(x,y,z) \qquad \text{Eq. 1}$$

2.1 Colinear transformation

if *n* (Refraction index in the object space) and *n'* (Refraction index in the image space) are constant the collinear transformation is a useful mathematical tool to approximate an imaging system. The general form of the linear transformation is given by:

$$x' = \frac{a_1x+b_1y+c_1z+d_1}{a_0x+b_0x+c_0x+d_0} \qquad \text{Eq. 2a}$$

$$y' = \frac{a_2x+b_2y+c_2z+d_2}{a_0x+b_0x+c_0x+d_0} \qquad \text{Eq. 2b}$$

$$z' = \frac{a_3x+b_3y+c_3z+d_3}{a_0x+b_0x+c_0x+d_0} \qquad \text{Eq. 2c}$$

Where at least one of the constant coefficients *a, b, c* and *d,* in the denominator is not 0. Equation 2 implies that a one to one relation exists between the object and the image space, as a consequence of that:

- Points in object space produce points in image space.
- Lines in object space produce lines in image space.
- Planes in object space produce planes in image space.
- An extended object formed by a collection of points in the object spaces produces and extended image formed by the superposition of the image of the object points

In the general form (Eq. 2) the collinear transformation has 16 coefficients, but if the equation is divided by one of the coefficients the total number of independent coefficients required is 15. 5 non coplanar image points with 3 spatial coordinates per point are required to find all the parameters of the transformation.

Equation 2 is used as starting point for the definition of general systems, eventually the number of parameters required to define the transformation are directly influenced by the symmetries of the system. Two particular cases will be studied in this chapter.

2.1.1 Rotational symmetric systems

The collinear transformation is the representation of the famous Gaussian and Newtonian equations (depending on the coordinate reference systems).

In the case of axial symmetry, a radial coordinate in the object and image can be defined by:

$$\rho = \sqrt{x^2 + y^2} \qquad \text{Eq. 3a}$$

$$\rho' = \sqrt{x'^2 + y'^2} \qquad \text{Eq. 3b}$$

The axial symmetry imposes 2 conditions:

- Planes normal to the axis of symmetry are imaged in planes normal to the axis of symmetry without distortion.
- The origin in the object space is mapped in the origin in the image space.

Because of these conditions, *ρ'* and *z'* are only functions of *ρ* and *z*. Consequently, some of the coefficients in Eq. 2. will turn to 0, and the collinear transformation equations for an axisymmetric system are reduced to

$$x' = \frac{a_1 x}{c_0 z + d_0} \qquad \text{Eq. 4a}$$

$$y' = \frac{b_2 y}{c_0 z + d_0} \qquad \text{Eq. 4b}$$

$$z' = \frac{c_3 z}{c_0 z + d_0} \qquad \text{Eq. 4c}$$

The coordinate system can be placed in the intersection between the plane of unit magnification (Principal Planes) and the symmetry axis (Figure 1). This convention in the coordinate system can be expressed in Eq 4 as:

- $x' = x$ When z=0
- $y' = y$ When z=0
- $z' = 0$ When z=0

That necessarily means: $a_1 = b_2 = d_0 = 1$ and $d_3 = 0$.

By the definition of the transverse magnification:

$$m = \frac{x'}{x} = \frac{y'}{y} = \frac{1}{c_0 z + 1} \qquad \text{Eq. 5}$$

The conjugation between the rear and the front focal points, with planes in the infinity in object and image planes in Eq. 4c implies:

$$for\ z = -\infty;\ z' = f' = \frac{c_3}{c_0} \qquad \text{Eq. 6a}$$

$$for\ z = -f;\ z' = \infty\ \therefore\ c_0 = \frac{1}{f} \qquad \text{Eq. 6b}$$

Replacing equations 6 and 5 in 4 the Gaussian equations that relate the object position, the image position, the focal lengths, and the magnification are obtained:

$$m = \frac{1}{1-\frac{z}{f}} \qquad \text{Eq. 7a}$$

$$m = 1 - \frac{z'}{f'} \qquad \text{Eq. 7b}$$

$$\frac{z'}{f'} - \frac{z}{f} = 1 \qquad \text{Eq. 7c}$$

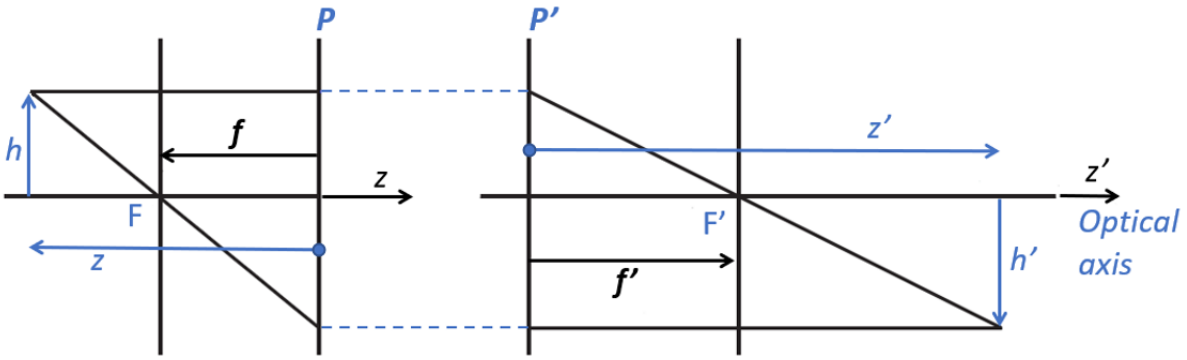

Figure 1 Coordinate system for Gaussian equations

Other convenient localization of the coordinate systems are the focal points. This specific case corresponds to the Newtonian equations:

$$\frac{z'}{f'} = m \qquad \text{Eq. 8b}$$

$$z \cdot z' = f \cdot f' \qquad \text{Eq. 8c}$$

2.1.2 Plane symmetric systems

For a system with plane symmetry in the *yz* (Figure 2) following conditions are established:

- *x'(x)= x'(-x), y'(x)= y'(-x)* and *z'(x)=z'(-x)* (plane symmetry)
- The coordinate origins must be conjugated so that *x'=y'=z'=0* when *x=y=z=0*
- The *z* axis must map into the *z'* axis.
- The plane of symmetry in image space must be the *y'-z'*
- The origins must be located so that *x'=x* when *y=z=0*.

After applying these conditions in Eq. 2 many coefficients are vanished and the resulting colinear transformation for plane symmetry is given by:

$$x' = \frac{x}{1+b_0 y+c_0 z} \qquad \text{Eq. 9a}$$

$$y' = \frac{b_2 y}{1+b_0 y+c_0 z} \qquad \text{Eq. 9b}$$

$$z' = \frac{c_3 z+b_3 y}{1+b_0 y+c_0 z} \qquad \text{Eq. 9c}$$

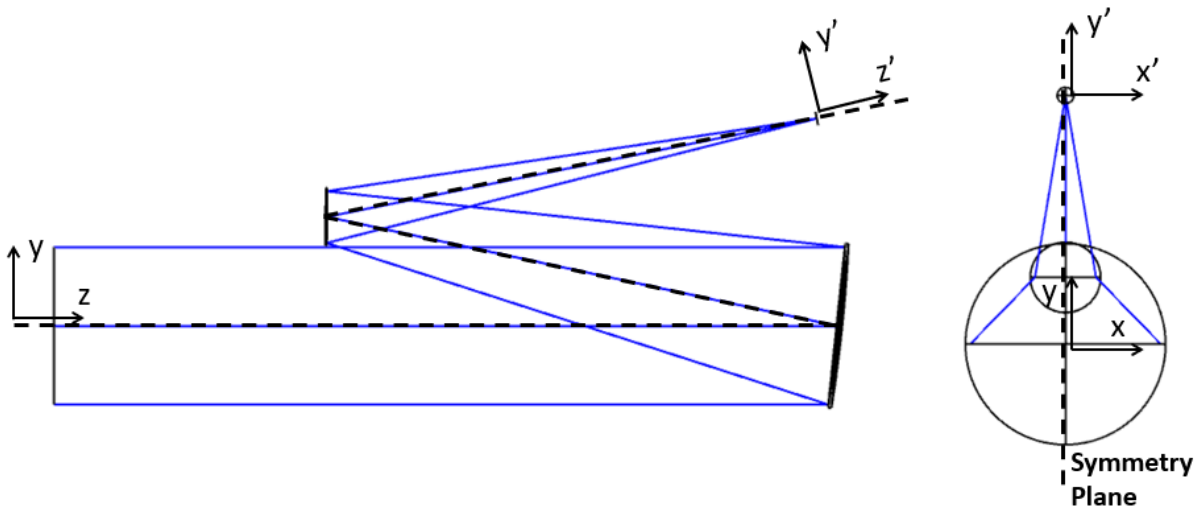

Figure 2 Schematic representation of a plane symmetric system

The derivation of equations akin to Gaussian equations for plane symmetry systems is substantially more complex. It involves the use of Coddington equations and more elaborated trigonometric relations. More details about this topic can be found in chapter 15 [1] and in the appendix section in [2] .

3 Imaging based on wave theory

A complete study about the interaction of an electromagnetic wave with the different components of an optical system is material complete book. in this chapter the basic concepts required to understand the propagation of electromagnetic waves in free space, the interaction of them with an aperture and the black box representation of a general optic system are revisited. This basic knowledge introduces the concept of pupil function as the output of an imaging system. The theoretical frame presented in the following paragraphs is based on [1], [3], and [4].

The Maxwell's equations describe the interaction between the electromagnetic disturbances and the matter. The starting point of this section are the Maxwell's equations in absence of free charge:

$$\nabla \times \vec{\mathcal{E}} = -\mu \frac{\partial \vec{\mathcal{H}}}{\partial t} \qquad \text{Eq. 10a}$$

$$\nabla \times \vec{\mathcal{H}} = -\epsilon \frac{\partial \vec{\mathcal{E}}}{\partial t} \qquad \text{Eq. 10b}$$

$$\nabla \cdot \epsilon \vec{\mathcal{E}} = 0 \qquad \text{Eq. 10c}$$

$$\nabla \cdot \mu \vec{\mathcal{H}} = 0 \qquad \text{Eq. 10d}$$

Where:

$\vec{\mathcal{E}}$: Electric field $\left(\mathcal{E}_x, \mathcal{E}_y, \mathcal{E}_z\right)$

$\vec{\mathcal{H}}$: Magnetic field $\left(\mathcal{H}_x, \mathcal{H}_y, \mathcal{H}_z\right)$

μ: Magnetic permeability of the medium

ε: Electric permittivity medium

∇: Nabla operator $=\frac{\partial}{\partial x}\hat{x} + \frac{\partial}{\partial y}\hat{y} + \frac{\partial}{\partial z}\hat{z}$

If the medium of propagation of the wave is: dielectric, linear, isotropic (the permittivity is independent of the direction of polarization of the wave), homogeneous (permittivity is constant in the propagation medium) nondispersive (permittivity is independent of the wavelength) and nonmagnetic (magnetic permeability is equal a μ_0) . After some manipulations between Maxwell's equations, it turns out that the electric and the magnetic fields must fulfil equations 12 and 13 respectively

$$\nabla^2 \vec{\mathcal{E}} - \left(\frac{n}{c}\right)^2 \frac{\partial^2 \vec{\mathcal{E}}}{\partial t^2} = 0 \qquad \text{Eq. 12}$$

$$\nabla^2 \vec{\mathcal{H}} - \left(\frac{n}{c}\right)^2 \frac{\partial^2 \vec{\mathcal{H}}}{\partial t^2} = 0 \qquad \text{Eq. 13}$$

Where the medium refraction index (*n*) is defined by:

$$n = \left(\frac{\epsilon}{\epsilon_0}\right) \qquad \text{Eq. 14}$$

And light speed in the vacuum is given by:

$$c = \frac{1}{\sqrt{\mu_0 \cdot \epsilon_0}} \qquad \text{Eq. 15}$$

The vectorial wave equations Eq. 12 and Eq 13 imply the same scalar relation for each component of the fields $\vec{\mathcal{E}}$ and $\vec{\mathcal{H}}$. or example for $\mathcal{E}_x$:

$$\nabla^2 \mathcal{E}_x - \left(\frac{n}{c}\right)^2 \frac{\partial^2 \mathcal{E}_x}{\partial t^2} \qquad \text{Eq. 16}$$

If Ω(x,y,z,t) is a scalar field that solves equations 12, 13 and 16, the vectorial equation and any scalar component of the field are summarized in:

$$\frac{\partial^2\Omega}{\partial x^2}+\frac{\partial^2\Omega}{\partial y^2}+\frac{\partial^2\Omega}{\partial z^2}=\left(\frac{n}{c}\right)^2\frac{\partial^2\Omega}{\partial t^2} \qquad \text{Eq. 17}$$

A possible set of solutions in separable variables of the scalar wave equation could be:

$$\Omega(x,y,z,t)=\psi(x,y,z)\cdot e^{\pm 2\pi i\nu t} \qquad \text{Eq. 18}$$

Where ν is the optical frequency. The function $\psi(x,y,z)$ is only function of the spatial variables. From the condition of separable variables in Eq. 17, it can be concluded that $\psi(x,y,z)$ must fulfil the time-independent equation:

$$\frac{\partial^2\psi}{\partial x^2}+\frac{\partial^2\psi}{\partial x^2}+\frac{\partial^2\psi}{\partial x^2}=-k^2\psi \qquad \text{Eq. 19}$$

The term *k* is known as the "wave number":

$$k=2\pi n\frac{\nu}{c}=\frac{2\pi}{\lambda} \qquad \text{Eq. 20}$$

The greek letter λ in Eq. 20 represents the wavelength in the dielectric medium. Equation 19 is known as the Helmholtz equation and is used to study propagation of electromagnetic and mechanical waves in uniform homogeneous mediums.

Three common solutions for the Helmholtz equation are:

- Plane wave:
  $p(x,y,z)=A_p e^{ik(\alpha x+\beta y+\gamma z)}$ Eq. 22
  Where α, β and γ are the direction cosine of the propagation direction

- Spherical wave:
  $s(x,y,z)=A_s\frac{e^{j\cdot k\sqrt{x^2+y^2+z^2}}}{\sqrt{x^2+y^2+z^2}}$ Eq. 23

- Oblique spherical wave or Pinhole wave
  $o(x,y,z)=A_o\frac{e^{j\cdot k\sqrt{x^2+y^2+z^2}}}{\sqrt{x^2+y^2+z^2}}\left(jk-\frac{1}{\sqrt{x^2+y^2+z^2}}\right)\frac{z}{\sqrt{x^2+y^2+z^2}}$
  for z>>λ
  $o(x,y,z)\cong\frac{A_o}{z}\frac{jkz^2}{(x^2+y^2+z^2)}e^{jk\sqrt{x^2+y^2+z^2}}$ Eq. 24

3.1.1 Apertures and scalar diffraction.

The formulation of a wave propagation is based on the original idea of the Dutch physicists Christiaan Huygens (1629 – 1695). For him each point in the wavefront of a disturbance was considered a new source of spherical waves, the wavefront at a later instant is defined by the envelope of the secondary wavelets, see Figure 3.

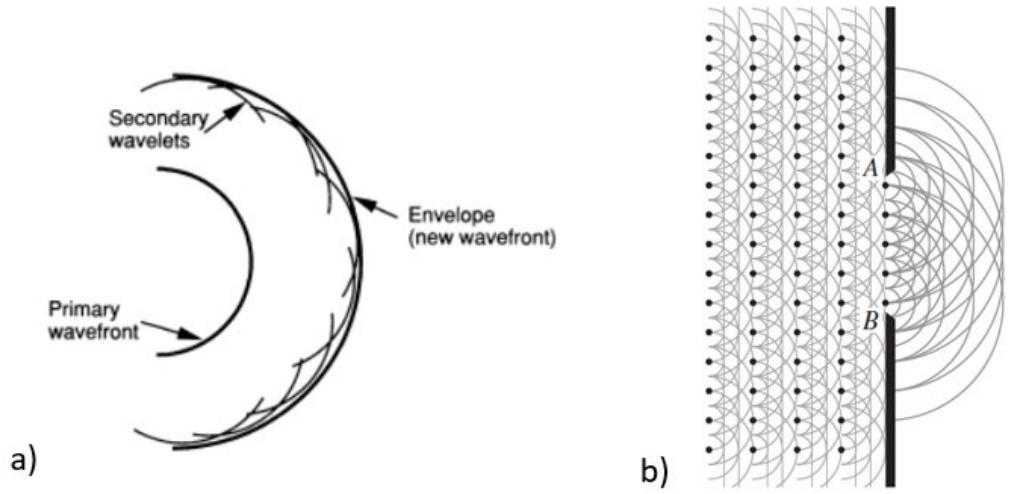

Figure 3 a) Huygens envelope construction in free space [3] b) Huygens's wavelet through a small aperture [5]

With some adjustments based in the interference theory proposed by Thomas Young, Fresnel propose a formal representation of the diffraction theory.

$$\psi(x,y,0)_s^+ = \psi(x,y,0)_s^- \cdot t_{ap}(x,y) \qquad \text{Eq. 27}$$

Where:

$\psi(x,y,0)_s^+$: Field after the aperture

$t_{ap}(x,y)$: Amplitude transmittance aperture function

$\psi(x,y,0)_s^-$: Field before the aperture

For example, the transmittance of a clear circular aperture is given by:

$$t_{ap}(x,y) = circ\left(2\frac{\sqrt{x^2+y^2}}{r_{ap}}\right) \qquad \text{Eq. 28}$$

A complete explanation of the propagation of the wave described by Eq. 27 is out of the scope of the report. Nevertheless, to present a complete frame of reference of aberration theory an overview of the diffraction phenomenon is required. The Figure 4 and Figure 5 [4] show a flow diagram summarizing how to deal with the propagation of waves in free space. In essence there are two different approaches that describe the diffraction phenomena. The right side of the diagram (Figure 4) shows the Free Space Point Spread Function (PSF) approach where the resulting electric field at the observation plane is calculated by integration of the individual response of the field in the aperture. Depending on the distance between the aperture (or source) and the plane of interest different approximations are valid. Rayleigh-Somerfield and Huygens are valid for the complete range of distance respect to the aperture (close, near, or far field), Fresnel approximation for near field and Fraunhofer approximation for far field. The terms "close to the aperture", "near field" and "far field" are stated by the Fresnel number N_f.

$$N_f = \frac{r_{ap}}{z.\lambda} \qquad \text{Eq. 29}$$

Each approximation has its own wavelet that model the input field, a complete description of the PSF method is summarized in Figure 5.

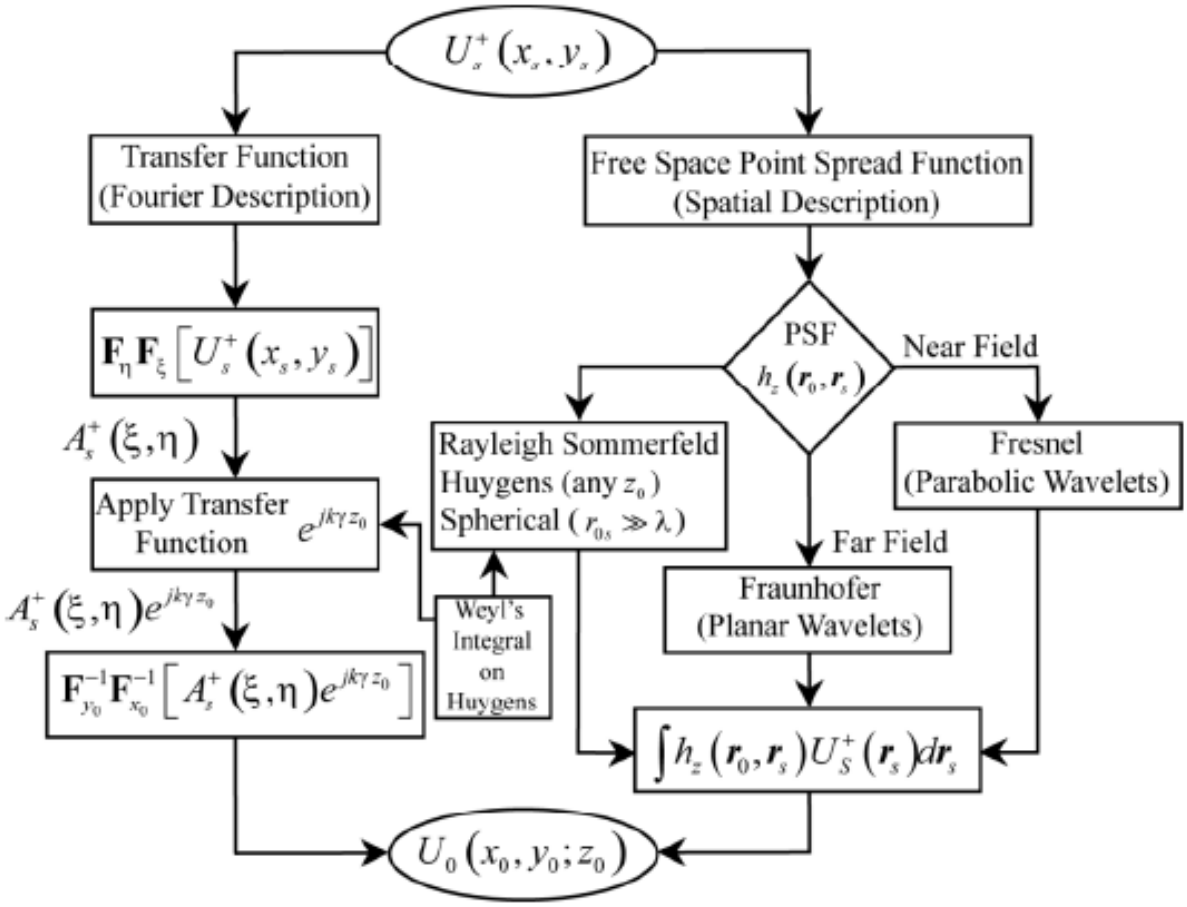

Figure 4 Diffraction flow diagram, including free space point spread function and transfer function approaches [4]

Diffraction as well as imaging systems can be modeled using the theory of linear shift invariant systems and the complete framework of the Fourier theory. Broadly speaking for a given perturbation at z_0, a system (including the free space, left branch in Figure 4) operates as a cascade of elements described in the Fourier domain by the transfer function. the image of one element is the object of the next element. In the space domain the response is the convolution of the perturbation and the impulse response function of the element, so form the convolution theorem, in the Fourier domain the response of the system is fully described by the product of the transfer function and the (angular) spectral representation of the input.

Figure 6 shows the main components of a physical imaging system. The object is illuminated by a light source, or it is self-emitting. The field at the object can be decomposed in a set of plane waves; then diffraction is considered using the Fourier theory and the concept of transfer function; finally, the intensity at the image plane is the time averaging of the electromagnetic waves transmitted through the system.

5.2.12 Summary of diffraction formulations

Table 5-4. Summary of diffraction formulations

Formulation	Equations	Range/Condition	Application
Rayleigh-Sommerfeld	Huygens $U_0(r_0)=\int_{ap}\left(\frac{-j}{\lambda}+\frac{1}{2\pi r_{0s}}\right)\gamma_s\frac{\exp(jkr_{0s})}{r_{0s}}U_s(r_s)dr_s$	All z_0	Planar aperture to general surface. Not often used in this form
	Circular Wavelet $U_0(r_0)=\frac{-j}{\lambda}\int_{ap}\gamma_s\frac{\exp(jkr_{0s})}{r_{0s}}U_s(r_s)dr_s$	$z_0\gg\lambda$	Planar aperture to general surface
Fresnel	$U_0(r_0)=\frac{-j\exp(jkz_0)}{\lambda z_0}\int_{ap}U_s(r_s)\times\exp\left[\frac{jk}{2z_0}\left[(x_0-x_s)^2+(y_0-y_s)^2\right]\right]dr_s$ or $U_0(r_0)=\frac{-j\exp(jkr_{0s})}{\lambda z_0}e^{\frac{jk}{2z_0}(x_0^2+y_0^2)}\int_{-\infty}^{\infty}U_s^+(r_s)\times\exp\left[j\frac{k}{2z_0}(x_s^2+y_s^2)\right]\exp\left[-j\frac{k}{z_0}(x_0x_s+y_{0s}y_s)\right]dr_s$	$z_0\gg\sqrt[3]{\frac{\pi}{4}}\lambda\left[\left(\frac{x_0-x_s}{\lambda}\right)^2+\left(\frac{y_0-y_s}{\lambda}\right)^2\right]$ or $\sim N_f<1000$	Planar aperture to planar observation screen.
Fraunhofer	$U_0(r_0)=\frac{-j\exp(jkz_0)}{\lambda z_0}\exp\left[\frac{jk}{2z_0}(x_0^2+y_0^2)\right]\int_{-\infty}^{\infty}U_s^+(r_s)\times\exp\left[-j\frac{k}{z_0}(x_0x_s+y_0y_s)\right]dr_s$	Must satisfy Fresnel and $z_0\gg\frac{k}{2}(x_s^2+y_s^2)_{max}$ or $\sim N_f<0.1$	Planar aperture to planar observation screen
Fresnel to a spherical surface	$U_0(\xi,\eta)=\frac{-j\gamma}{\lambda r}\mathbf{F}_{\eta\to\frac{\beta}{\lambda}}\mathbf{F}_{\xi\to\frac{\alpha}{\lambda}}\left\{U_s^+(r_s)\exp\left[j\frac{k}{2r}(x_s^2+y_s^2)\right]\right\}$	$r\gg x_s$ $r\gg y_s$ $r\gg\lambda$	Planar aperture to sphere centered on aperture vertex (See

Figure 5 Summary of diffraction PSFs and distance of validity [Ref 4]

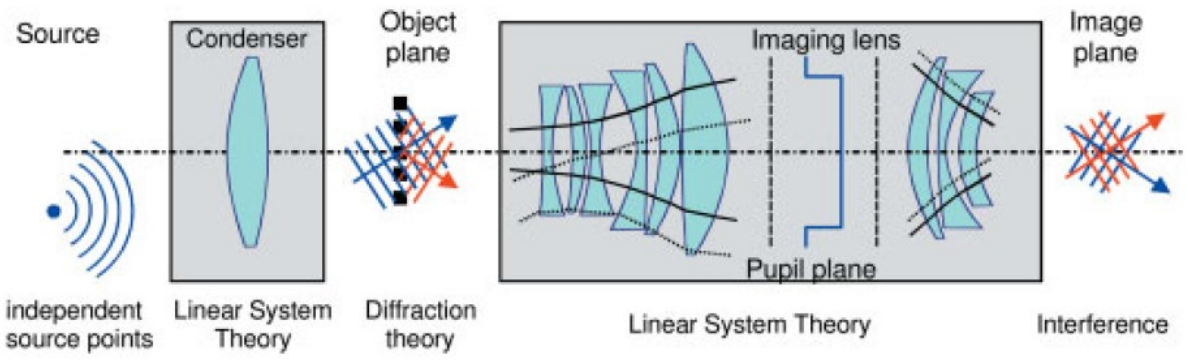

Figure 6 Physical model of a optical imaging system [Ref. 6]

One way to model a system is thinking of the system as black box that maps the entrance pupil into the exit pupil. In a perfect system the relation between both pupils is described by geometrical optics.

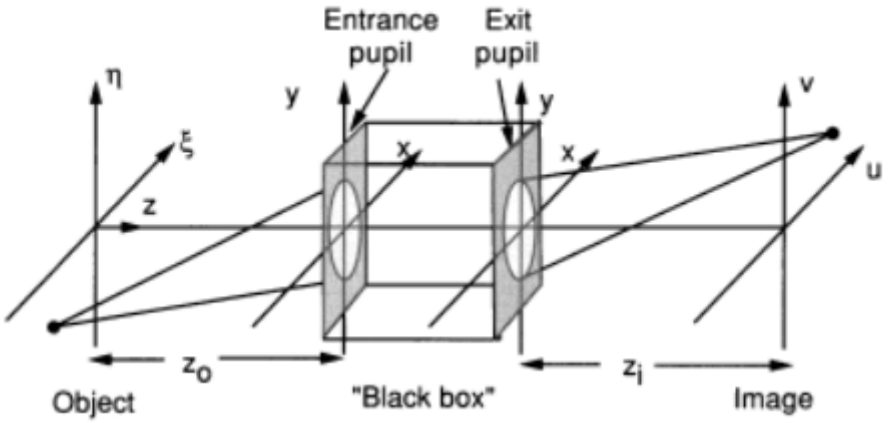

Figure 7 Generalized Model of an Imaging System [Ref 3]

In Figure 7, the distances z_o and z_i represent the distances between the object and the entrance pupil and the distance between the exit pupil and the image plane.

In geometrical optics a system produces stigmatic images: all the rays from an object point intersect in the same ideal point at the image plane as it is described in section 2. In the physical world the best performance of an optical system is physically limited by diffraction. Goodman in [3] provides the next definition for diffraction limited systems and its characteristics:

"An imaging system is said to be diffraction-limited if a diverging spherical wave, emanating from a point-source object, is converted by the system into a new wave, again perfectly spherical, that converges towards an ideal point in the image plane, where the transverse location of that ideal image point is related to the transverse location of the original object point through a simple scaling factor (the magnification), a factor that must be the same for all points in the image field of interest if the system is to be ideal… For any real imaging system, this property will be satisfied, at best, over only finite regions of the object and image plane. If the object of interest is confined to the region for which this property holds, then the system may be regarded as being diffraction limited"

In Figure 7 we have defined an object coordinate system *(ξ,η)* and image coordinate system *(u,v)*. The formulation of the Fourier optics for incoherent illumination has established:

$$I_i(u,v) = \kappa \iint_{-\infty}^{\infty} \left|h\left(u-\tilde{\xi}, v-\tilde{\eta}\right)\right|^2 \cdot I_g\left(\tilde{\xi},\tilde{\eta}\right) d\tilde{\xi} d\tilde{\eta} \qquad \text{Eq. 30}$$

Equation 30 is key result. The *"image intensity"* I_i is the result of the convolution of the *"intensity impulse response"* $|h(u,v)|^2$ with the *"ideal image intensity"* $I_g\left(\tilde{\xi},\tilde{\eta}\right)$.

Where $h(u,v)$ is the response from a spherical wave converging from the exit pupil:

$$h\left(u-\tilde{\xi}, v-\tilde{\eta}\right) = \frac{1}{\lambda^2 z_i^2} \iint_{-\infty}^{\infty} P(x,y) \cdot e^{-j\frac{2\pi}{\lambda z_i}\left[(u-\tilde{\xi})x+(v-\tilde{\eta})y\right]} dx \cdot dy \qquad \text{Eq. 31}$$

P(x,y) is the pupil function; for a diffraction limited system it is 1 inside the exit pupil aperture and 0 otherwise.

Using the convolution theorem, equation 30 can be written in the spatial frequency domain as:

$$\mathcal{G}_i(f_X, f_Y) = \mathcal{H}(f_X, f_Y) \cdot \mathcal{G}_g(f_X, f_Y) \quad \text{Eq. 32}$$

Where $\mathcal{G}_g(f_X, f_Y)$ and $\mathcal{G}_i(f_X, f_Y)$ are the normalized spectra of I_g and I_i:

$$\mathcal{G}_g(f_X, f_Y) = \frac{\iint_{-\infty}^{\infty} I_g(u,v) \cdot e^{-2\pi j(f_X u + f_Y v)} du dv}{\iint_{-\infty}^{\infty} I_g(u,v) du dv} \quad \text{Eq. 33}$$

$$\mathcal{G}_i(f_X, f_Y) = \frac{\iint_{-\infty}^{\infty} I_i(u,v) \cdot e^{-2\pi j(f_X u + f_Y v)} du dv}{\iint_{-\infty}^{\infty} I_i(u,v) du dv} \quad \text{Eq. 34}$$

$\mathcal{H}(f_X, f_Y)$ is the *Optical Transfer Function* (OTF) defined by:

$$\mathcal{H}(f_X, f_Y) = OTF = \frac{\iint_{-\infty}^{\infty} |h(u,v)|^2 \cdot e^{-2\pi j(f_X u + f_Y v)} du dv}{\iint_{-\infty}^{\infty} |h(u,v)|^2 du dv} \quad \text{Eq. 35}$$

$$MTF = |OTF| \quad \text{Eq. 36}$$

The modulus of the OTF is known as the "Modulation Transfer Function" (MTF), equation 36. It is an important indicator of the image quality of a system used extensively in chapter 5.

4 Wavefront aberration

In the previous chapter a diffraction limited system was define as a system which in presence of a point source produces a perfect spherical wave converging from the exit pupil towards the image point. This ideal wavefront is represented in Figure 8 by the Gaussian reference sphere. If the wavefront emerging from the exit pupil (Actual wavefront in Figure 8) departs substantially from the Gaussian spherical wavefront the system is aberrated. Aberrations are commonly modelled as phase errors, to introduce them in the linear model described in previous chapter it is useful to define a new general pupil function P_w:

$$P_w(x,y) = P(x,y) \cdot e^{j \cdot k \cdot W(x,y)} \qquad \text{Eq. 37}$$

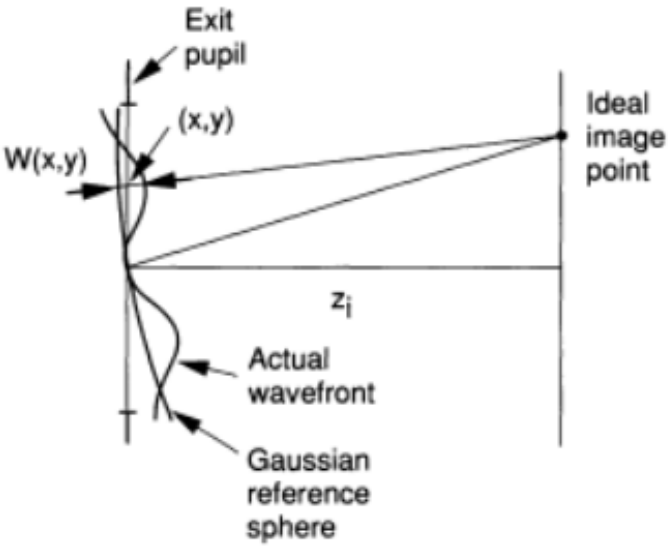

Figure 8 Gaussian reference sphere and aberrated wavefront at the exit pupil [Ref 3]

The amplitude of the point spread function in the image point in an aberrated system would be understood as the Fraunhofer (Figure 4 and Figure 5) diffraction pattern of an aperture with amplitude and phase transmittance defined by the real pupil function P_w. The consequence of the aberrations for real systems is well described in [3]:

"Thus, aberrations cannot increase the contrast of any spatial-frequency component of the image, and in general will lower the contrast. The absolute cutoff frequency remains unchanged, but severe aberrations can reduce the high-frequency portions of the OTF to such an extent that the effective cutoff is much lower than the diffraction-limited cut off.

Both effects described in the previous paragraph can be observed in Figure 9.

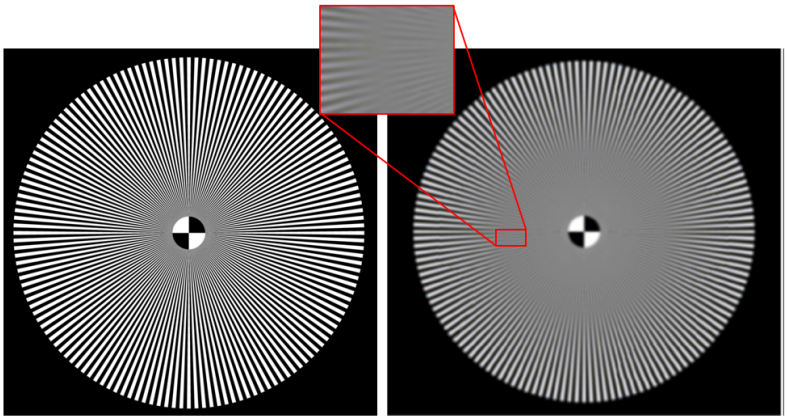

Figure 9 Spoke target and the aberrated image (result from HW5 OPTI 503)

4.1 Axisymmetric Systems

In the entire discussion presented in section 3 axial symmetry was subjacent: Circular apertures, point sources with spherical waves, spherical waves converging from a circular pupil. It is a natural consequence of the axial symmetry that for a point source on-axis the image point is an axisymmetric blurred spot. For off-axis points the situation is different: The pupil is no longer normal to the chief ray. As a consequence, the chief ray, the tangential ray and the sagittal ray do not focus on the same point as we can see in Figure 10 (Illustration of the formation of coma aberration). The blurred spot is no longer symmetric with respect to the sampling in the pupil (Figure 10 a), but the field sampling shows how the aberration pattern is symmetric in the field of view with respect to the optical axis (Figure 10 b)

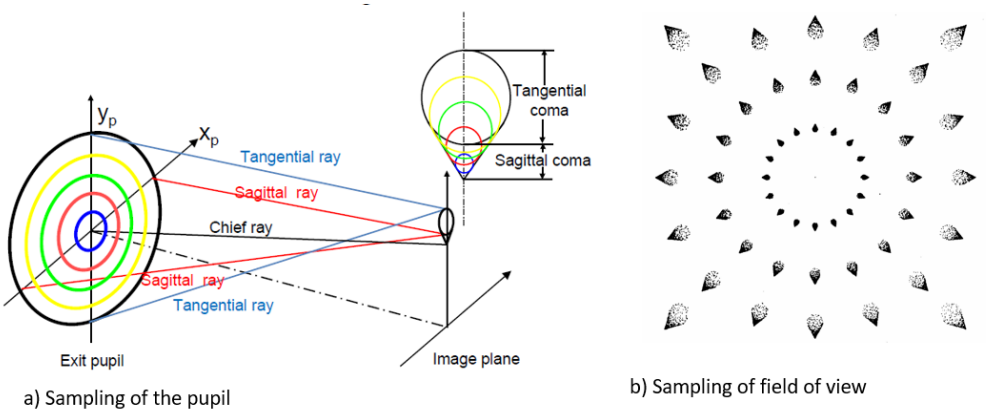

Figure 10 Off axis image point a) sampling of the pupil, b) Sampling of the field of view [6]

In the representation of the system in Figure 7, a point in the object plane produce and spherical wavefront cone that fills the complete entrance pupil, then this wavefront is transferred and magnified to the exit pupil and after collapses in the image point. The same transformation from the object point to the image point using rays is shown in Figure 10 and Figure 11. Where the Gaussian or first order ray, represented by the broken line is associated to the Gaussian sphere, and the real ray, represented by the solid line is associated the actual wavefront. For each ray we can define two vectors: The normalized aperture vector($\vec{\rho}$ (x_p,y_p)) and the normalized field vector ($\vec{H}(H_x,H_y)$). The aperture vector has its foot in the optical axis and can be placed either in the entrance or the exit pupil. The field vector has its foot in the optical axis and can be placed in either the object or the image plane. The angle between both vectors in a plane normal to the optical axis is ϕ.

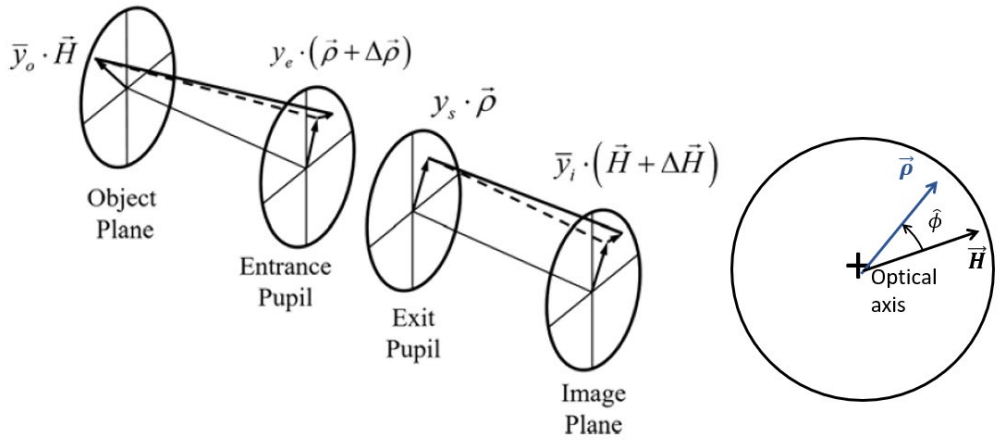

Figure 11 Gaussian ray (broken line) and real ray (solid) line in an optical system [7]

A practical approach to represent the wavefront aberration function *W(x,y)* is based in power series, using the axisymmetric condition. It turns out that W(x,y) can be expressed as a power series of $(\vec{H} \cdot \vec{H})$, $(\vec{H} \cdot \vec{\rho})$ and $(\vec{\rho} \cdot \vec{\rho})$:

$$W(\vec{H}, \vec{\rho}) = \sum_{j,m,n} W_{k,l,m} (\vec{H} \cdot \vec{H})^j (\vec{H} \cdot \vec{\rho})^m (\rho \cdot \rho)^n \qquad \text{Eq. 37}$$

$$(\vec{H} \cdot \vec{H}) = H^2 \qquad \text{Eq. 38}$$

$$(\vec{\rho} \cdot \vec{\rho}) = \rho^2 \qquad \text{Eq. 39}$$

$$(\vec{H} \cdot \vec{\rho}) = H\, \rho\, cos(\varphi) \qquad \text{Eq. 40}$$

The sub-indices *j, m, n* are integers and the coefficients $W_{k,l,m}$ are the aberration coefficient that weight the shapes defined by the vectorial products: $(\vec{H} \cdot \vec{H})^j (\vec{H} \cdot \vec{\rho})^m (\rho \cdot \rho)^n$. The subindex in the wavefront aberration coefficients are given by:

$$k = 2j + m \qquad \text{Eq. 41}$$

$$l = 2n + m \qquad \text{Eq. 42}$$

Using equations 37 to 42 the wavefront aberration function can be written in algebraic form. Table 1 is a summary of the wavefront aberration function till the sixth order. It includes the vector and the algebraic forms. The table is divided by horizontal bars associated with the order defined by the summation of the exponents of *H* and *ρ* in the algebraic form. The names of the aberration in many cases includes the order of the dependence of the aberration with the field coordinate, for example W_{131} is "linear" coma and W_{331} is "cubic" coma. A detailed description of the shapes of the aberrations for each order is presented in Figure 12, Figure 13, Figure 14, Figure 15, and Figure 16.

From Table 1 and Figure 12 to Figure 16 it can be seen how, for each $2*n^{th}$ order the aberrations of the previous $2*(n-1)^{th}$ order aberration are scaled by H2 and (n+1) new aberrations appears.

Table 1 Wavefront aberration for axisymmetric systems

Aberration name and order	Vector form	Alegebraic form	j	m	n	k	l
Zero Order							
Uniform Piston	W_{000}	W_{000}	0	0	0	0	0
Second Order							
Defocus	$W_{020}(\vec{\rho}\cdot\vec{\rho})$	$W_{020}\,\rho^2$	0	0	1	0	2
Magnification	$W_{111}(\vec{H}\cdot\vec{\rho})$	$W_{111}H\,\rho\cos(\varphi)$	0	1	0	1	1
Quadratic Piston	$W_{200}(\vec{H}\cdot\vec{H})$	$W_{200}H^2$	1	0	0	2	0
Fourth Order							
Spherical Aberration	$W_{040}(\vec{\rho}\cdot\vec{\rho})^2$	$W_{040}\rho^4$	0	0	2	0	4
Linear Coma	$W_{131}(\vec{H}\cdot\vec{\rho})(\vec{\rho}\cdot\vec{\rho})$	$W_{131}H\,\rho^3\cos(\varphi)$	0	1	1	1	3
Astigmatism	$W_{222}(\vec{H}\cdot\vec{\rho})^2$	$W_{222}H^2\,\rho^2\,cos^2(\varphi)$	0	2	0	2	2
Field Curvature	$W_{220}(\vec{H}\cdot\vec{H})(\vec{\rho}\cdot\vec{\rho})$	$W_{220}H^2\,\rho^2$	1	0	1	2	2
Distortion	$W_{311}(\vec{H}\cdot\vec{H})(\vec{H}\cdot\vec{\rho})$	$W_{311}H^3\,\rho\cos(\varphi)$	1	1	0	3	1
Quartic Piston	$W_{400}(\vec{H}\cdot\vec{H})^2$	$W_{400}H^4$	2	0	0	4	0
Sixth Order							
Oblique Spherical A.	$W_{240}(\vec{H}\cdot\vec{H})(\vec{\rho}\cdot\vec{\rho})^2$	$W_{240}H^2\,\rho^4$	1	0	2	2	4
Cubic Coma	$W_{331}(\vec{H}\cdot\vec{H})(\vec{H}\cdot\vec{\rho})(\vec{\rho}\cdot\vec{\rho})$	$W_{331}H^3\,\rho^3\cos(\varphi)$	1	1	1	3	3
4th Astigmatism	$W_{422}(\vec{H}\cdot\vec{H})(\vec{H}\cdot\vec{\rho})^2$	$W_{422}H^4\,\rho^2\,cos^2(\varphi)$	1	2	0	4	2
Field Curvature	$W_{420}(\vec{H}\cdot\vec{H})^2(\vec{\rho}\cdot\vec{\rho})$	$W_{420}H^4\,\rho^2$	2	0	1	4	2
Distortion	$W_{511}(\vec{H}\cdot\vec{H})^2(\vec{H}\cdot\vec{\rho})$	$W_{511}H^5\,\rho\cos(\varphi)$	2	1	0	5	1
Piston	$W_{600}(\vec{H}\cdot\vec{H})^3$	$W_{600}H^6$	3	0	0	6	0
Spherical Aberration	$W_{060}(\vec{\rho}\cdot\vec{\rho})^3$	$W_{060}\rho^6$	0	0	3	0	6
Secondary Coma	$W_{151}(\vec{H}\cdot\vec{\rho})(\vec{\rho}\cdot\vec{\rho})^2$	$W_{151}H\,\rho^5\cos(\varphi)$	0	1	2	1	5
Secondary Astigm.	$W_{242}(\vec{H}\cdot\vec{\rho})^2(\vec{\rho}\cdot\vec{\rho})$	$W_{242}H^2\,\rho^4\,cos^2(\varphi)$	0	2	1	2	4
Arrows [Ref 8]	$W_{333}(\vec{H}\cdot\vec{\rho})^3$	$W_{422}H^3\,\rho^3\,cos^3(\varphi)$	0	3	0	3	3

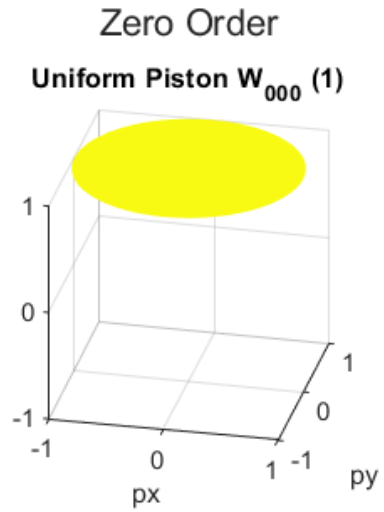

Figure 12 Zero order group

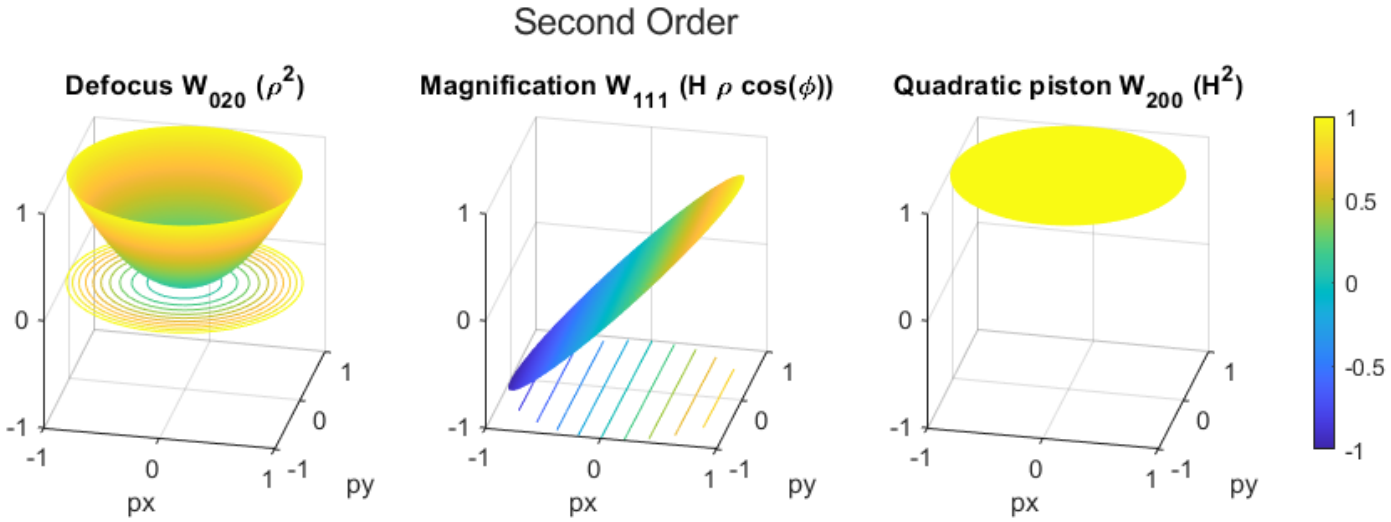

Figure 13 Second order group

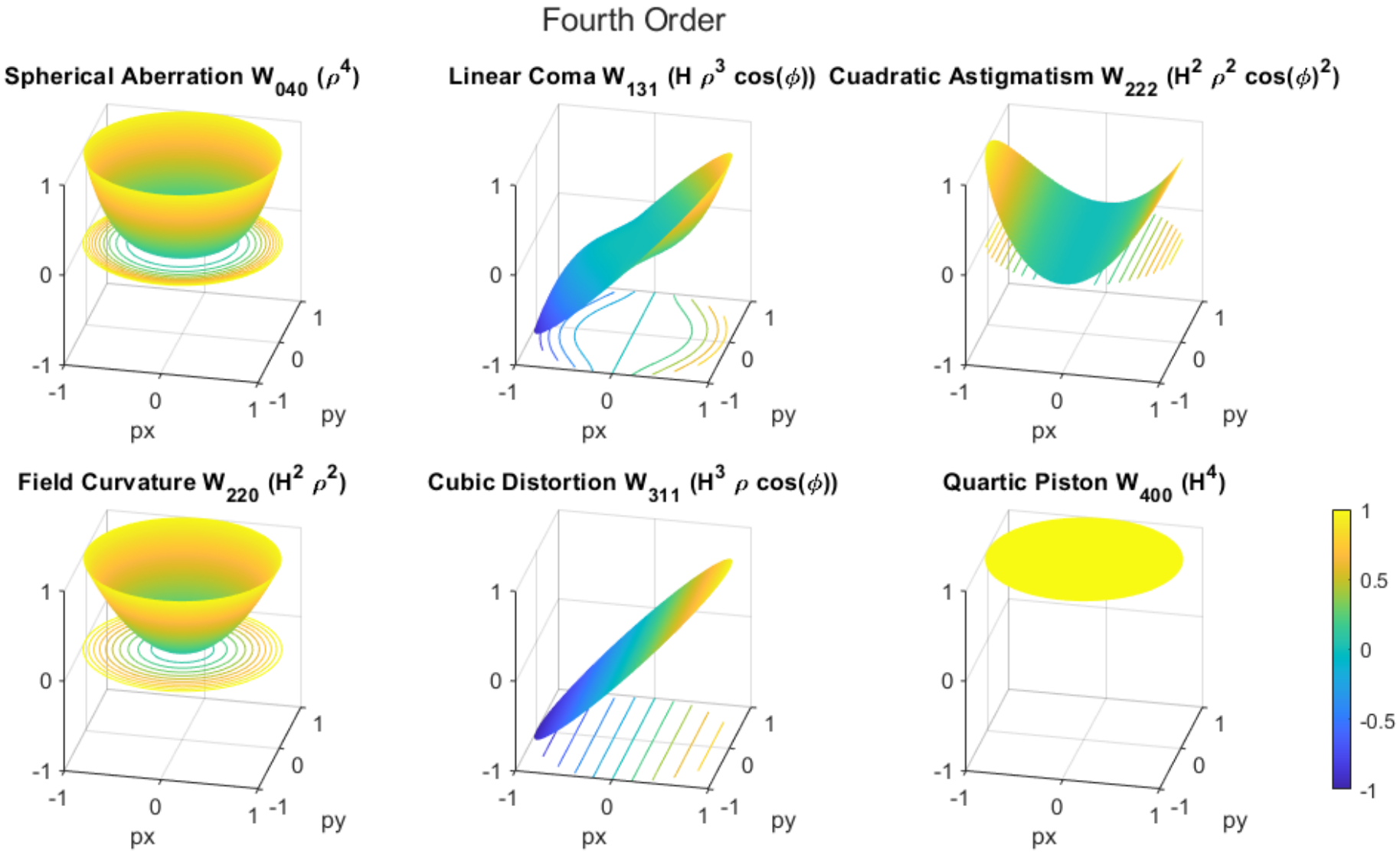

Figure 14 Fourth Order group

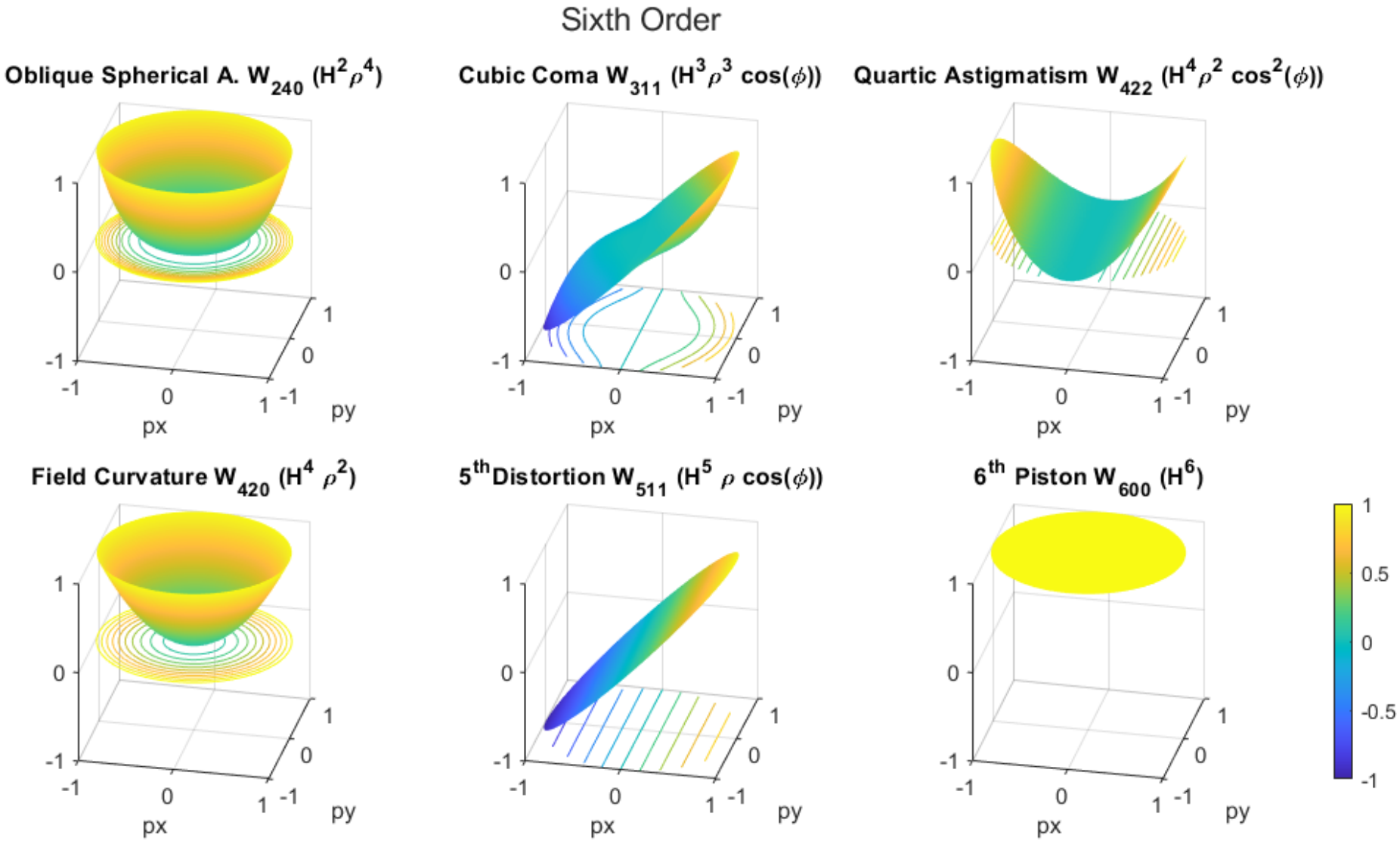

Figure 15 Sixth Order group (common aberrations with 4th order group)

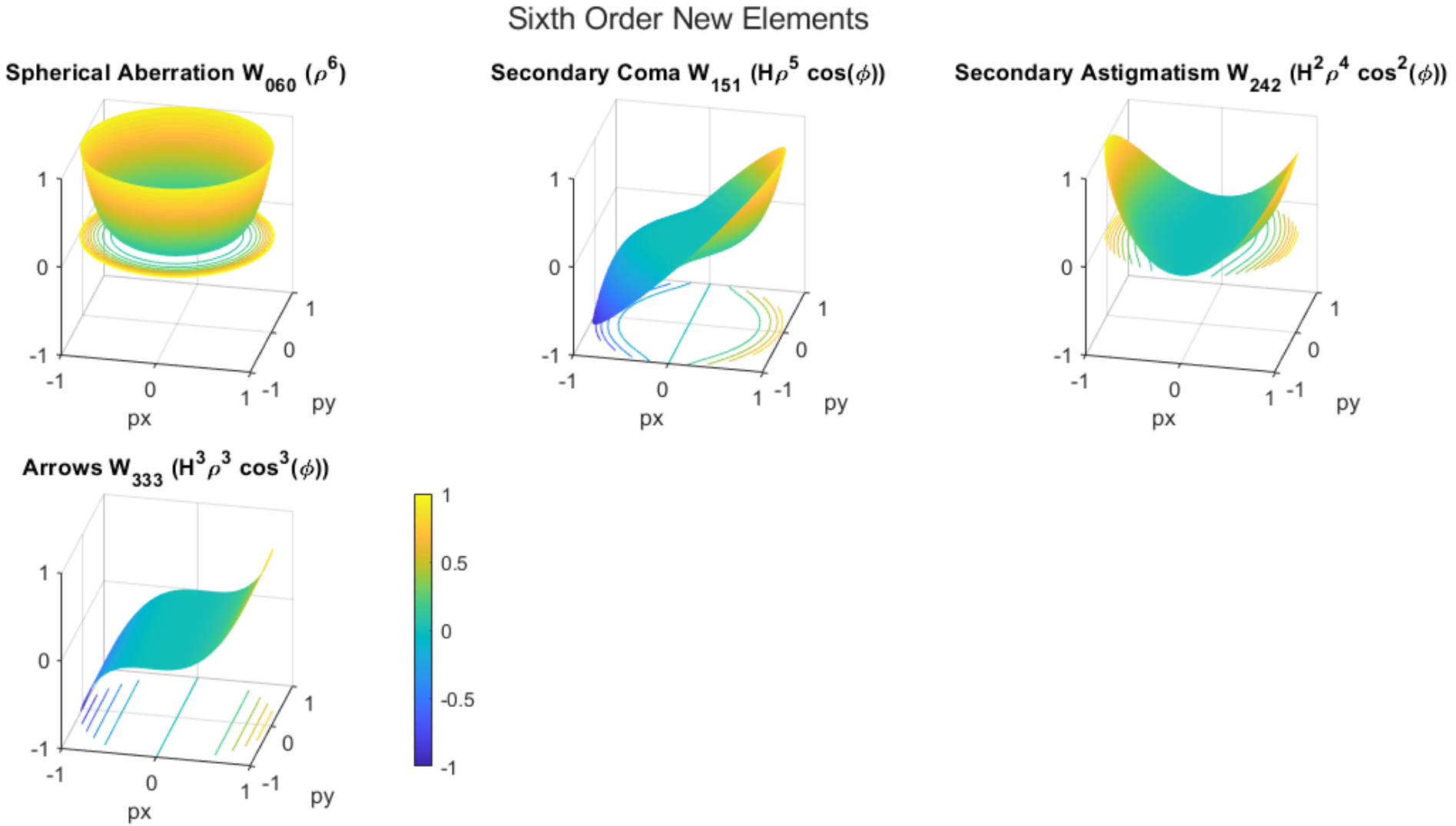

Figure 16 Sixth Order group (New Elements)

In practice the piston terms do not degrade the performance of the system, they are a phase delay in the wavefront. The second order terms W_{111} and W_{020} are associated with the magnification and the axial position of the image plane. Because the Gaussian equation provides good information about the magnification and the position of the image plane, these terms are not considered aberrations. Even more, often some defocus is deliberately induced in a system to partially correct other aberrations.

4.1.1 Wavefront Aberration Coefficients

The aberration coefficients till fourth order, also called primary aberrations can be calculated using Seidel sums, These sums are functions of:

- Field of view
- Aperture
- Refraction indexes
- Surface curvature
- Surface separation
- Asphericity
- Stop position

A quite remarkable feature of the Seidel sums is the fact that all the information required for the calculation of the sums is contained in the ray tracing of the marginal and chief rays (geometric optics), the curvatures, and the refraction index of the media. The Table 2 show the wavefront coefficients ($W_{\#\#\#}$) in terms of the Seidel sums ($S_{\#}$). The index in the summation operator (Σ) represent the surfaces in the optical system

Table 2 Wavefront aberration Coefficients and Seidel Sums

Aberration	Coefficient	Seidel Sum
Spherical Aberration $\boldsymbol{W_{040}(\vec{\rho}\cdot\vec{\rho})^2}$	$W_{040} = \frac{1}{8}S_I$	$S_I = -\sum_{i=1}^{j}\left(A^2 y\Delta\left(\frac{u}{n}\right)\right)_i$
Linear Coma $\boldsymbol{W_{131}(\vec{H}\cdot\vec{\rho})(\vec{\rho}\cdot\vec{\rho})}$	$W_{131} = \frac{1}{2}S_{II}$	$S_{II} = -\sum_{i=1}^{j}\left(A\bar{A}y\Delta\left(\frac{u}{n}\right)\right)_i$
Astigmatism $\boldsymbol{W_{222}(\vec{H}\cdot\vec{\rho})^2}$	$W_{222} = \frac{1}{2}S_{III}$	$S_{III} = -\sum_{i=1}^{j}\left(\bar{A}^2 y\Delta\left(\frac{u}{n}\right)\right)_i$
Field Curvature $\boldsymbol{W_{220}(\vec{H}\cdot\vec{H})(\vec{\rho}\cdot\vec{\rho})}$	$W_{220} = \frac{1}{2}(S_{IV} + S_{III})$	$S_{IV} = -\aleph^2\sum_{i=1}^{j}P_i$
Distortion $\boldsymbol{W_{311}(\vec{H}\cdot\vec{H})(\vec{H}\cdot\vec{\rho})}$	$W_{220} = \frac{1}{2}S_V$	$S_V = -\sum_{i=1}^{j}\left(\frac{\bar{A}}{A}\left(\aleph^2 P + \bar{A}y\Delta\left(\frac{u}{n}\right)\right)\right)_i$
Chromatic change of focus $\boldsymbol{\delta_\lambda W_{020}}$	$\boldsymbol{\delta_\lambda W_{020}} = \frac{1}{2}C_L$	$C_L = \sum_{i=1}^{j}\left(Ay\Delta\left(\frac{\delta n}{n}\right)\right)_i$
Chromatic change of magnification $\boldsymbol{\delta_\lambda W_{111}}$	$\boldsymbol{\delta_\lambda W_{111}} = C_T$	$C_T = \sum_{i=1}^{j}\left(\bar{A}y\Delta\left(\frac{\delta n}{n}\right)\right)_i$

Where:

Refraction Invariant marginal ray:	$A = ni = nu + nyc$	Eq. 43
Refraction Invariant chief ray:	$\bar{A} = n\bar{\imath} = n\bar{u} + n\bar{y}c$	Eq. 44
Lagrange Invariant:	$\aleph = n\bar{u}y - nu\bar{y} = \bar{A}y - A\bar{y}$	Eq. 45
Surface curvature:	$c = {}^{1}/_{r}$	Eq. 46
Petzval sum term:	$P = c \cdot \Delta\left(\frac{1}{n}\right) = c\left(\frac{1}{n'} - \frac{1}{n}\right)$	Eq. 47
	$\Delta\left(\frac{u}{n}\right) = \left(\frac{u'}{n'} - \frac{u}{n}\right)$	Eq. 48

The last two rows in Table 2 are chromatic aberrations generated by the wavelength dispersion in dioptric systems. The first order aberrations induced by dispersion are: Change of focus ($\boldsymbol{\delta_\lambda W_{020}}$) and chromatic change of magnification ($\boldsymbol{\delta_\lambda W_{111}}$). The operator $\Delta\left(\frac{\delta n}{n}\right)$ is associated to the change of refraction index in the surface. As illustrative example, if a system is working in the visible FdC spectrum the operator $\Delta\left(\frac{\delta n}{n}\right)$ is given by:

$$\Delta\left(\frac{\delta n}{n}\right) = \frac{\delta n'}{n'} - \frac{\delta n}{n}; \qquad \delta n = n_F - n_C \text{ and } n = n_d$$

4.1.2 Aspheric surfaces contribution

One way to visualize an aspheric surface is to imagine a spherical surface with an aspherical cap. The sag (Z_{asph}) for this surface till fourth order is defined by the conic constant and the coefficient A_4:

$$Z_{asph} = \frac{1}{2r}(x^2 + y^2) + \frac{1}{8r^3}(1 + K)(x^2 + y^2)^2 + A_4(x^2 + y^2)^2 \qquad \text{Eq. 49}$$

Where:

r: is the radius at the vertex of the surface
K: is the conic constant. For conic surface $-\varepsilon^2$(ε is the eccentricity)
A_4: Fourth Coefficient

The parameter *"a"* associated to the contribution of the aspheric surface in the Seidel sums depends on the way the aspheric surface is defined:

For conic constant surfaces:

$$a = -\varepsilon^2 c^3 y^4 \Delta(n) \qquad \text{Eq. 50}$$

For fourth-order coefficient surfaces:

$$a = 8A_4 y^4 \Delta(n) \qquad \text{Eq. 51}$$

The contributions of the aspheric contribution to the Seidel coefficients are:

$$\delta S_I = a \qquad \text{Eq. 52}$$

$$\delta S_{II} = \left(\frac{\bar{y}}{y}\right) a \qquad \text{Eq. 53}$$

$$\delta S_{III} = \left(\frac{\bar{y}}{y}\right)^2 a \quad \text{Eq. 54}$$

$$\delta S_{IV} = 0 \quad \text{Eq. 55}$$

$$\delta S_{V=} \left(\frac{\bar{y}}{y}\right)^3 a \quad \text{Eq. 56}$$

$$\delta C_L = 0 \quad \text{Eq. 57}$$

$$\delta C_T = 0 \quad \text{Eq. 58}$$

As we can see in Eq. 55, 57 and 58 the contribution of the 4th order aspheric surfaces to the field curvature and chromatic aberrations is 0.

Aspheric surfaces are an effective way of correcting spherical aberration when they are placed close to the stop or pupils. When the aspheric surface is placed far from the pupils it has a strong effect in astigmatism and distortion. Unfortunately, both effects occur simultaneously. For this reason, it is common to use the aspheric surface to control distortion and use lens bending for the astigmatism.

4.1.3 Stop Shifting

From Table 1 and equations 43 to 45 in section 4.1.1 we can see the dependency of the wavefront aberration coefficient of the optical invariants and eventually to the height and slope of the marginal and chief rays. All these variables are strongly connected with the position of the stop in the system. The stop shifting parameter is given by:

$$\bar{S} = \frac{\bar{u}_{new} - \bar{u}_{old}}{u} = \frac{\bar{y}_{new} - \bar{y}_{old}}{y} = \frac{\bar{A}_{new} - \bar{A}_{old}}{A} \quad \text{Eq. 59}$$

The slope and the height of the marginal ray do not change with the stop shifting, so the refraction invariant changes only for the chief ray, in the equations 61 to 67 the symbol (*) represents values after the stop shifting:

$$\bar{A}_{new} = \bar{A}_{old} + \bar{S}A \quad \text{Eq. 60}$$

The Seidel sums after stop shifting are given by equations 61 to 67.

$$S_I^* = S_I \quad \text{Eq. 61}$$

$$S_{II}^* = S_{II} + \bar{S}S_I \quad \text{Eq. 62}$$

$$S_{III}^* = S_{III} + 2\bar{S}S_{II} + \bar{S}^2 S_I \quad \text{Eq. 63}$$

$$S_{IV}^* = S_{IV} \quad \text{Eq. 64}$$

$$S_V^* = S_V + \bar{S}(S_{IV} + 3S_{III}) + 3\bar{S}^2 S_{II} + \bar{S}^3 S_I \quad \text{Eq. 65}$$

$$C_L^* = C_L \quad \text{Eq. 66}$$

$$C_T^* = C_T + \bar{S}C_L \quad \text{Eq. 67}$$

As it is expected all the aberrations that are independent of the chief ray are unalerted: Spherical aberration, field curvature and chromatic change of focus, equation 61, 64 and 66.

The position of the stop has also influence in the apertures of the elements and vignetting, so all these elements must be considered during the optimization process.

4.2 Plane symmetry systems

The study of plane symmetric systems has a relevant importance in modern optic design because, it allows to understand the behavior of systems that have lost the axial symmetry due to manufacturing and assembly tolerance. Another important application is the design of reflecting systems that avoid the central obscuration (Figure 18) inherent to the on-axis reflecting system (Figure 17), including a wide variety of devices such as: tilted-component telescope, microlithography systems, etcetera .

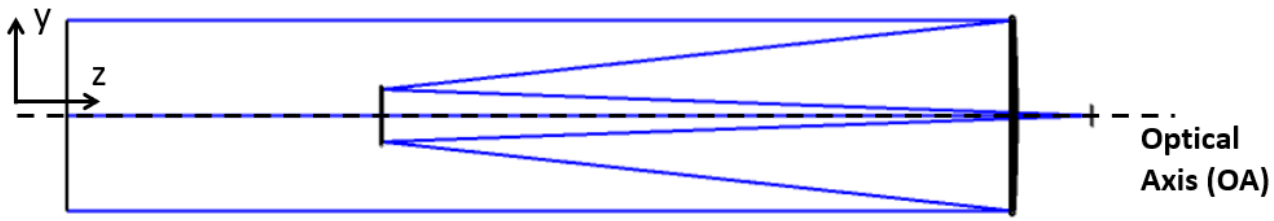

Figure 17 On-axis reflective telescope (with obscuration)

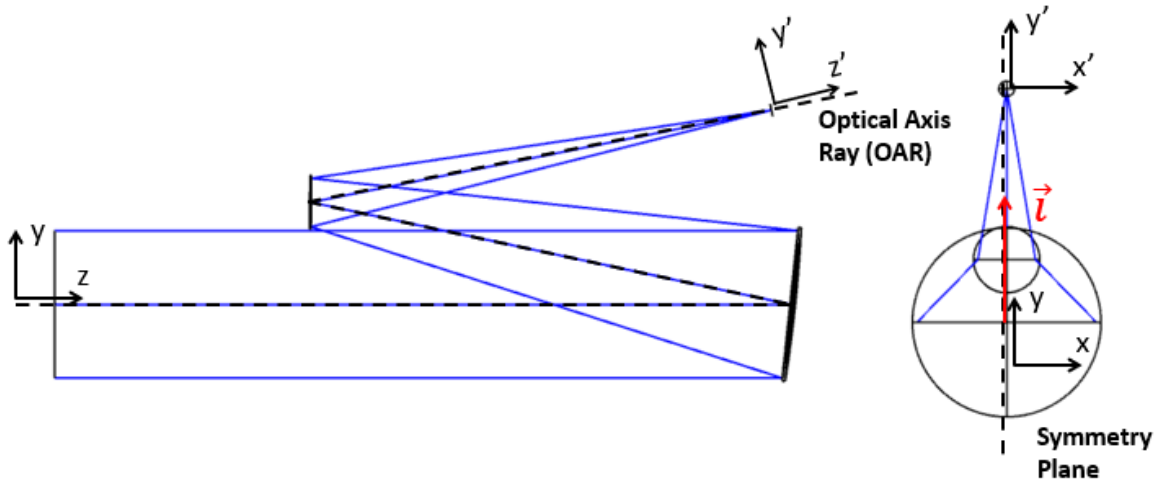

Figure 18 Tilted mirror telescope (without obscuration)

Section 2.1.2 introduces plane symmetry systems from the point of view of collinear transformation. This section we will go into further details and describes the wavefront aberration function for such systems. The methodology used in this section is described in deep in [2] and [8].

In axisymmetric systems the reference for the vectors involved in the description of the wavefront aberration functions is the Optical Axis (Figure 17). A similar reference is required in plane symmetry systems (Figure 18). The "Optical Axis Ray" (OAR) is contained in the symmetry plane and provides a frame of reference for the normalized aperture vector ($\vec{\rho}$) and the normalized field vector ($\vec{H}$).

The OA(R), $\vec{H}$, $\vec{\rho}$ are common elements between axisymmetric and the plane symmetry systems, but when the condition of axisymmetric is broken, a new vector that fixes the relative position between $\vec{H}$ and $\vec{\rho}$ and the plane of symmetry, is needed. This new entity is the vector ($\vec{\iota}$) that lies in the plane of symmetry and has its foot in the OAR. It is represented in Figure 18 by the red arrow.

Now all the necessary elements to define a wavefront aberration function akin to equation 37 are in place. As in the case of axisymmetric systems it is a scalar field , but for plane symmetric systems it depends on the

combination of the dot products between the normalized aperture vector ($\vec{\rho}$), the normalized field vector ($\vec{H}$) and the symmetry unit vector ($\vec{\imath}$). The new wavefront aberration $W(\vec{H},\vec{\rho},\vec{\imath})$ has the form:

$$W(\vec{H},\vec{\rho},\vec{\imath}) = \sum_{k,m,n,p,q}^{\infty} W_{2k+n+p,2m+n+q,n,p,q} (\vec{H}\cdot\vec{H})^{k} (\vec{\rho}\cdot\vec{\rho})^{m} (\vec{H}\cdot\vec{\rho})^{n} (\vec{\imath}\cdot\vec{H})^{p} (\vec{\imath}\cdot\vec{\rho})^{q} \quad \text{Eq. 68}$$

Where the dot products in equation 68 are:

$$\vec{H}\cdot\vec{H} = H^2 \quad \text{Eq. 69}$$
$$\vec{\rho}\cdot\vec{\rho} = \rho^2 \quad \text{Eq. 70}$$
$$\vec{H}\cdot\vec{\rho} = H\rho\cos(\phi) \quad \text{Eq. 71}$$
$$\vec{\imath}\cdot\vec{H} = H\,cos(\alpha) \quad \text{Eq. 72}$$
$$\vec{\imath}\cdot\vec{\rho} = \rho\,cos(\beta) \quad \text{Eq. 73}$$

The relation between the vectors $\vec{H}$, $\vec{\rho}$ and $\vec{\imath}$, and the angles α, β and ϕ is shown in Figure 19.

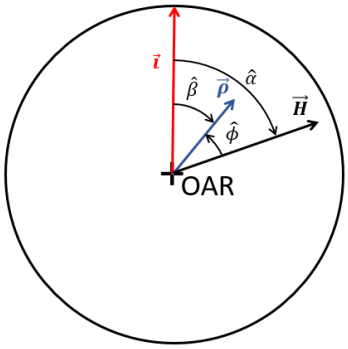

Figure 19 Field, aperture and symmetry unit vector and their angles

The wavefront aberration functions generated by variating the indexes in equation 68 are presented in Table 3. The first column lists the name of the aberration. The words linear, quadratic, etcetera are related with the power of *H* in the algebraic form. The coefficients are coded in the form $W_{2k+n+p,2m+n+q,n,p,q}$. The subindexes represent the power of *H, ρ, cos(ϕ), cos(α), cos(β)* in the algebraic form. The last 5 columns correspond with the values of the indexes k, m, n, p, q.

The observation of the last two indexes provides a clear idea of the symmetry of the wavefront aberration in the field of view. When p=q=0, the wavefront aberration function is symmetric with respect to the OAR. They are highlighted in blue in Table 3 and coincide with the aberrations in Table 1. When p+q=1, the wavefront aberration is strictly plane symmetric; these terms are highlighted in orange. Finally, when the p+q=2 the wavefront aberrations have double plane symmetry; those are the green lines in Table 3.

The different types of symmetries are schematically represented in Figure 20 (axisymmetric), Figure 21 (single plane symmetry) and Figure 22 (doble plane symmetry).

Table 3 Wavefront aberrations for axisymmetric systems

Aberration name and Group	Vector form	Algebraic form	k	m	n	p	q
First Group							
Constant Piston	W_{00000}	W_{00000}	0	0	0	0	0
Second Group							
Field Displacement	$W_{01001}(\vec{\imath}\cdot\vec{\rho})$	$W_{01001}\,\rho\cos(\beta)$	0	0	0	0	1
Linear Piston	$W_{10010}(\vec{\imath}\cdot\vec{H})$	$W_{10010}\,H\cos(\alpha)$	0	0	0	1	0
Defocus	$W_{02000}(\vec{\rho}\cdot\vec{\rho})$	$W_{02000}\,\rho^2$	0	1	0	0	0
Magnification	$W_{11100}(\vec{H}\cdot\vec{\rho})$	$W_{11100}\,H\rho\,\cos(\phi)$	0	0	1	0	0
Quadratic Piston	$W_{20000}(\vec{H}\cdot\vec{H})$	$W_{20000}\,H^2$	1	0	0	0	0
Third Group							
Constant Astigmatism	$W_{02002}(\vec{\imath}\cdot\vec{\rho})^2$	$W_{02002}\,\rho^2\,cos^2(\beta)$	0	0	0	0	2
Anamorphism	$W_{11011}(\vec{\imath}\cdot\vec{H})(\vec{\imath}\cdot\vec{\rho})$	$W_{11011}H\rho\cos(\alpha)\cos(\beta)$	0	0	0	1	1
Quadratic Piston	$W_{20020}(\vec{\imath}\cdot\vec{H})^2$	$W_{20020}\,H^2\,cos^2(\alpha)$	0	0	0	2	0
Constant Coma	$W_{03001}(\vec{\rho}\cdot\vec{\rho})(\vec{\imath}\cdot\vec{\rho})$	$W_{03001}\rho^3\cos(\beta)$	0	1	0	0	1
Linear Astigmatism	$W_{12101}(\vec{H}\cdot\vec{\rho})(\vec{\imath}\cdot\vec{\rho})$	$W_{12101}H\rho^2\cos(\beta)\cos(\phi)$	0	0	1	0	1
Field tilt	$W_{12010}(\vec{\rho}\cdot\vec{\rho})(\vec{\imath}\cdot\vec{H})$	$W_{12010}H\,\rho^2\,cos^2(\alpha)$	0	1	0	1	0
Quadratic Distortion I	$W_{21001}(\vec{H}\cdot\vec{H})(\vec{\imath}\cdot\vec{\rho})$	$W_{21001}H^2\rho\cos(\beta)$	1	0	0	0	1
Quadratic Distortion II	$W_{21110}(\vec{H}\cdot\vec{\rho})(\vec{\imath}\cdot\vec{H})$	$W_{21110}\,H^2\rho\cos(\alpha)\cos(\phi)$	0	0	1	1	0
Cubic Piston II	$W_{30010}(\vec{H}\cdot\vec{H})(\vec{\imath}\cdot\vec{H})$	$W_{30010}H^3\,cos^2(\alpha)$	1	0	0	1	0
Spherical Aberration	$W_{04000}(\vec{\rho}\cdot\vec{\rho})^2$	$W_{04000}\rho^4$	0	2	0	0	0
Linear Coma	$W_{13100}(\vec{H}\cdot\vec{\rho})(\vec{\rho}\cdot\vec{\rho})$	$W_{13100}H\,\rho^3\cos(\phi)$	0	1	1	0	0
Quadratic Astigmatism	$W_{22200}(\vec{H}\cdot\vec{\rho})^2$	$W_{22200}H^2\,\rho^2\,cos^2(\phi)$	0	0	2	0	0
Field Curvature	$W_{22000}(\vec{H}\cdot\vec{H})(\vec{\rho}\cdot\vec{\rho})$	$W_{22000}H^2\,\rho^2$	1	1	0	0	0
Cubic Distortion	$W_{31100}(\vec{H}\cdot\vec{H})(\vec{H}\cdot\vec{\rho})$	$W_{311000}H^3\,\rho\cos(\phi)$	1	0	1	0	0
Quartic Piston	$W_{40000}(\vec{H}\cdot\vec{H})^2$	$W_{40000}H^4$	2	0	0	0	0

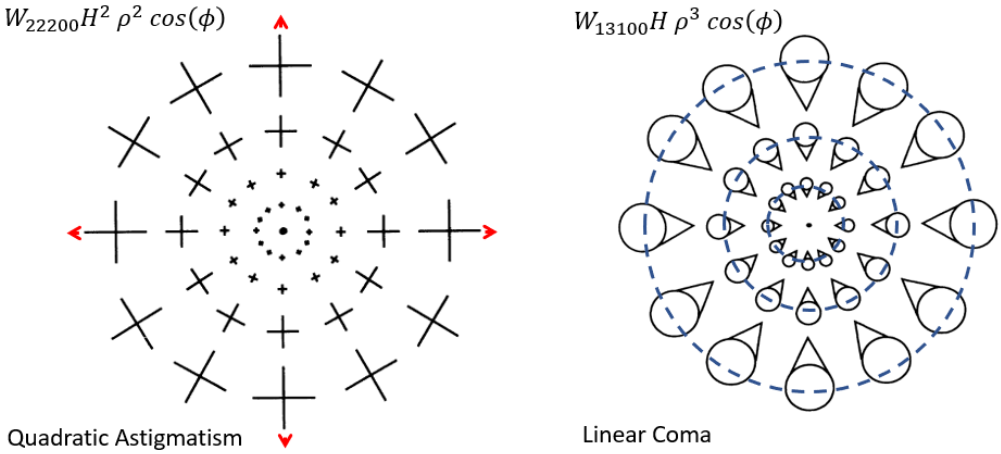

Figure 20 Schematic representation of two axisymmetric aberrations (adapted form [2])

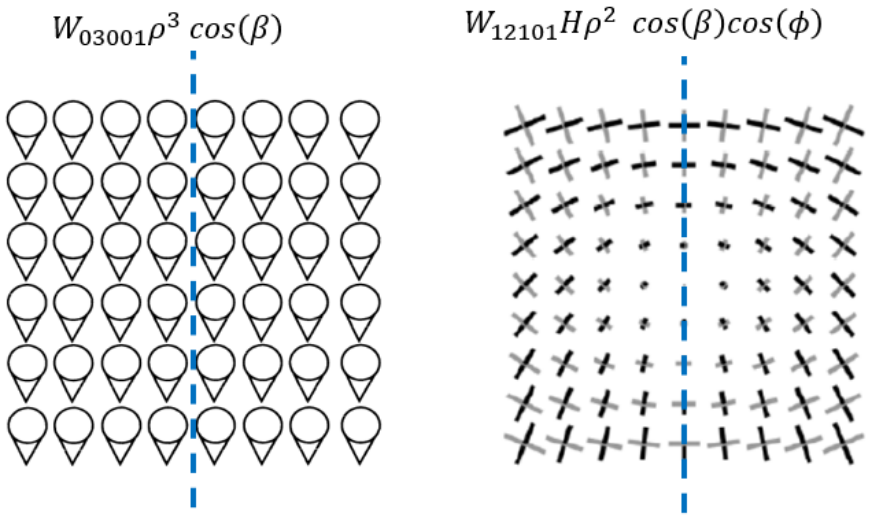

Figure 21 Schematic representation of constant coma and linear astigmatism two aberrations with only planar symmetry (adapted form [2])

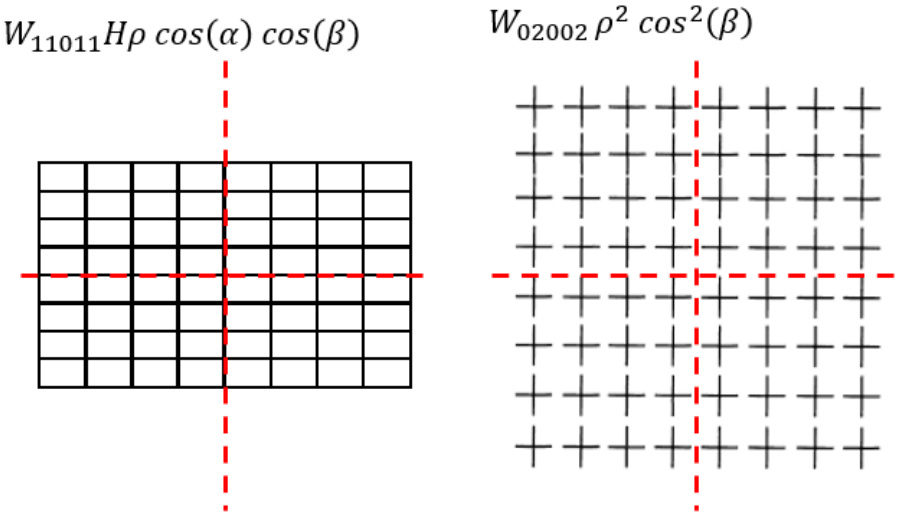

Figure 22 Schematic representation of anamorphism and constant astigmatism tow aberrations with double planar symmetry (adapted form [2])

In [2] there are expressions to calculate the wavefront aberration coefficients. For the work presented in chapter 5, only a clear visualization of the shape, the symmetry and the order of the aberrations is needed due to the surfaces selected to compensate the different aberrations terms.

5 Design of an unobscured telescope.

This section is based on the independent study carried out as requirement for the Master. The objective is designing a "Tilted Component Telescope" (TCT) which, inherent to its construction, presents plane symmetric aberrations. In the coming sections a strategy, introduced in [8], that allows the correction of aberration till 4th order, in plane symmetric systems, using freeform surfaces will be implemented. The design and optimization were done using Zemax OpticStudio V21.2.

The starting point is a Cassegrain on-axis telescope shown in Figure 23. Highlighted in green are the main characteristics of the system: The aperture is 1200 mm and F/# is 12. The wavefront aberration and the wavefront aberration coefficients for this configuration are shown in Figure 24.

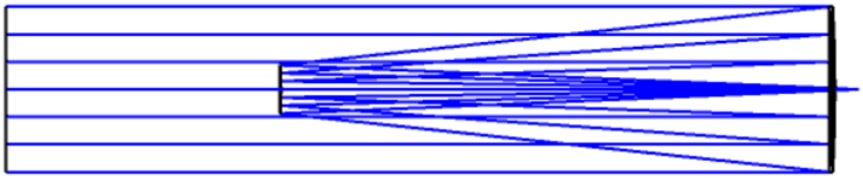

	Surface Type		Comme	Radius		Thickness	Material	Semi-Diameter
0	OBJECT	Standard		Infinity		Infinity		0.000
1		Standard		Infinity		5000.000		600.000 U
2		Coordinate Break				0.000	-	0.000
3	STOP (aper)	Standard		-1.132E+04	V	0.000	MIRROR	600.000 U
4		Coordinate Break				-4000.000	-	0.000
5		Coordinate Break				0.000	-	0.000
6		Standard		-5481.220	V	0.000	MIRROR	175.714
7		Coordinate Break				4200.000	-	0.000
8	IMAGE	Standard		Infinity		-		0.466

ISFN	12.000	10.000	11.988

Figure 23 Initial on axis telescope configuration.

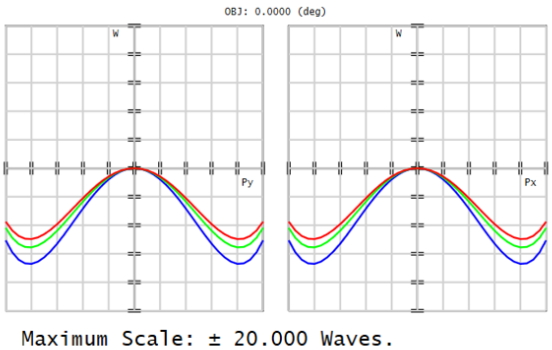

Maximum Scale: ± 20.000 Waves.

Wavefront Aberration Coefficient Summary:

	W040	W131	W222	W220P	W311	W020	W111
TOT	24.8483	0.0000	0.0000	0.0000	0.0000	0.0000	0.0000

	W220S	W220M	W220T
TOT	0.0000	0.0000	0.0000

Figure 24 Wavefront aberration and Wavefront aberration coefficient on axis telescope

Now the tilt in the primary mirror to avoid the obscuration and more points in the field of view are included. A first optimization using the tilt of the secondary mirror as variable was executed. The main characteristics of this telescope are shown in Figure 25. The wavefront aberration fans, and the spot diagrams are shown in Figure 26

and Figure 27, respectively. Both diagrams show a strong presence of coma aberration that is constant in the whole field of view. Figure 28, Shows the grid distortion: Two patterns symmetric with respect to the vertical plane can be identified. The red lines and arrows describe a keystone distortion meanwhile the green arcs represent a smile distortion pattern.

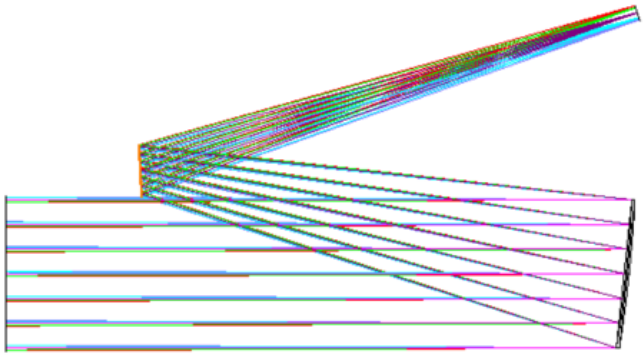

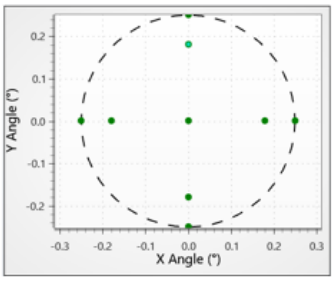

	Surface Type	Comment	Thickness	Radius	Semi-Diameter	Conic	Tilt About X
0	OBJI Standard		Infinity	Infinity	Infinity	0.0...	
1	Standard		5000.000	Infinity	626.761	0.0...	
2	Coordinate Break		0.000		0.000		6.000
3	STO Standard	Primary	0.000	-13526.090 V	600.000 U	0.0...	
4	Coordinate Break		-4000....		0.000		6.000 P
5	Coordinate Break		0.000		0.000		-15.994 V
6	Standard	Secondary	0.000	-16123.630 V	276.611	0.0...	
7	Coordinate Break		4200.000		0.000		-15.994 P
8	IMA Standard		-	Infinity	48.624	0.0...	

Figure 25 Tillted component telescope based on spherical surfaces

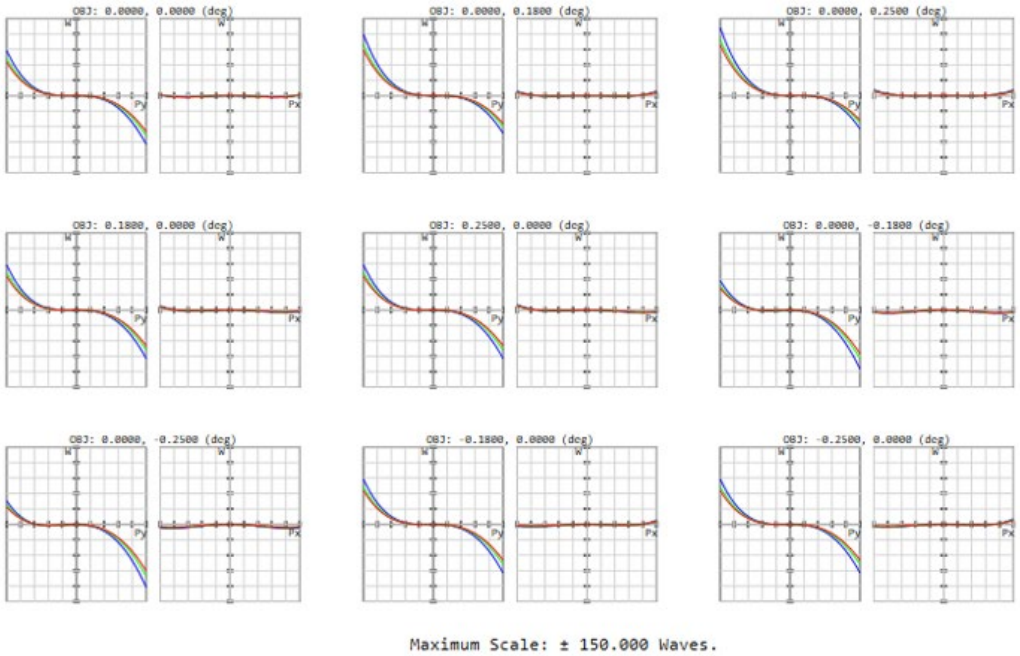

Figure 26 Wavefront aberration fans for a tilted component telescope based on spherical surfaces

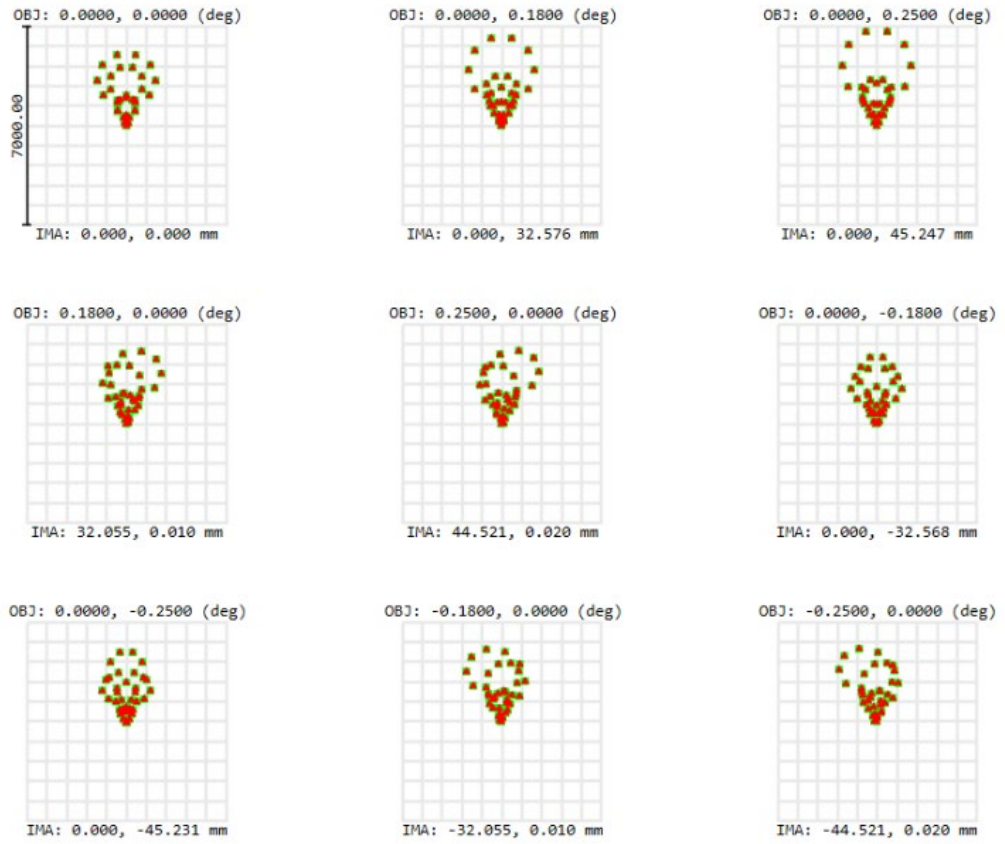

Figure 27 Wavefront aberration fans for a tilted component telescope based on spherical surfaces

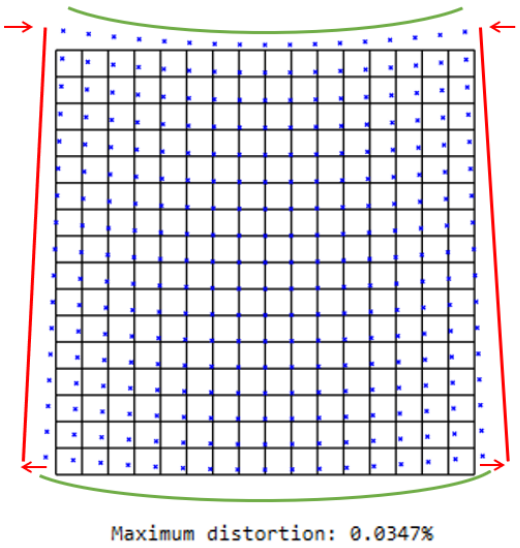

Figure 28 Grid distortion for a tilted component telescope based on spherical surfaces

In section 4.2 the shape, the symmetry, and the field dependence of the aberration wavefront function in plane symmetric systems were described. Three kinds of symmetry were identified: axial, double plane and "single" plane. The TCT presented in Figure 25 has at least two of these kinds of aberrations: The axial aberration inherent to the Cassegrain design and the plane symmetric constant coma introduced after the tilting of the mirrors. It seems logical that introducing surfaces that can deal with these aberrations is an effective strategy to optimize the system as it is suggested in [8]:

"… Thus the aberration properties of a symmetric system can be thought of as the superposition of the properties of axial, double plane and plane symmetric systems. The correction of the aberration of a given subgroup can be carried out using system properties according to subgroup symmetry. For example using a freeform surface having axial Z_α, double plane Z_β or plane Z_γ. Mathematically, these aspheric terms are:

$$Z_\alpha = \alpha(\vec{\rho}.\vec{\rho})^2 \qquad \text{Eq. 74}$$

$$Z_\beta = \beta(\vec{\rho}\cdot\vec{\iota}) \qquad \text{Eq. 75}$$

$$Z_\gamma = \gamma(\vec{\iota}\cdot\vec{\rho})(\vec{\rho}\cdot\vec{\rho}) \qquad \text{Eq. 76}$$

where α, β and γ are the aspheric coefficients."

There are many types of surfaces that meet the conditions from equations 74, 75 and 76. One of them is the Extended Polynomial Surface included in OpticStudio, its surface sag is of the form:

$$z = \left[\frac{c.r^2}{1+\sqrt{1-(1+k)c^2r^2}}\right] + \left[\sum_{i=1}^{n} A_i E_i(x,y)\right] \qquad \text{Eq. 77}$$

Where:

A_i: Coefficients of the ith extended polynomial

E_i: Power series expansion polynomial in the form $x^m y^n$

c: Curvature

k: Conic constant (k<-1 hyperbola, k=-1 parabolas, -1<k<0 for ellipses, k=0 for spheres and k>0 for oblate ellipsoids)

In Eq. 77, the expression in the first square bracket is an axisymmetric conic surface equivalent to the Eq. 74. The expression in the second bracket allows a power expansion for the aspheric surfaces associated to the equations 75 and 76. The first 15 terms of the power expansion in Eq. 77 are shown in Figure 29. The polynomials are identified with the label *Pmn* where the indexes *m* and *n* correspond to the powers of *x* and *y* respectively. The green (✓) tick marks identify the polynomial with double symmetry associated with Eq. 75 meanwhile the blue (✓) tick marks check the polynomials with only symmetry in the xz plane associated to equation 76.

From the results in Figure 24, Figure 26 and Figure 27 the presence of spherical aberration associated to the spherical mirrors and a strong component of constant coma have been established, a good first step for the optimization will be switching the mirror surface to extended polynomial surfaces and then set as variable the conic constant and the polynomials x^0y^3 for both mirrors. Figure 30 shows the result obtained, the constant coma has been reduced by a factor of 3 compared to Figure 26.

The wavefront aberration in Figure 30 is still dominated by the constant coma, the other polynomial in Figure 29 with single plane symmetry is x^2y. The wavefront aberration resulting after including this polynomial is shown in Figure 31. The uniform coma is totally removed and now the dominant aberration is linear astigmatism. The red rectangles in the field label identify the field point in the *y* axis, the wavefront aberration fan in these points have a parabolic profile and the curvature of these profiles vary linearly with the field.

The most convenient polynomial from Figure 29 to control the wavefront aberration in Figure 31 is P20. After releasing this degree of freedom in both mirrors, the wavefront aberration is dominated by higher order terms as can be seen in Figure 32. The surfaces prescription data for this design is shown in Figure 33, the variables used for the optimization are identified with the same colour code as in Table 3. The conic constant in blue for compensation of the axisymmetric aberrations, X0Y3 and X2Y1 in orange for the compensation of the single plane symmetry and X2Y0 for the compensation of the aberrations with double plane symmetry.

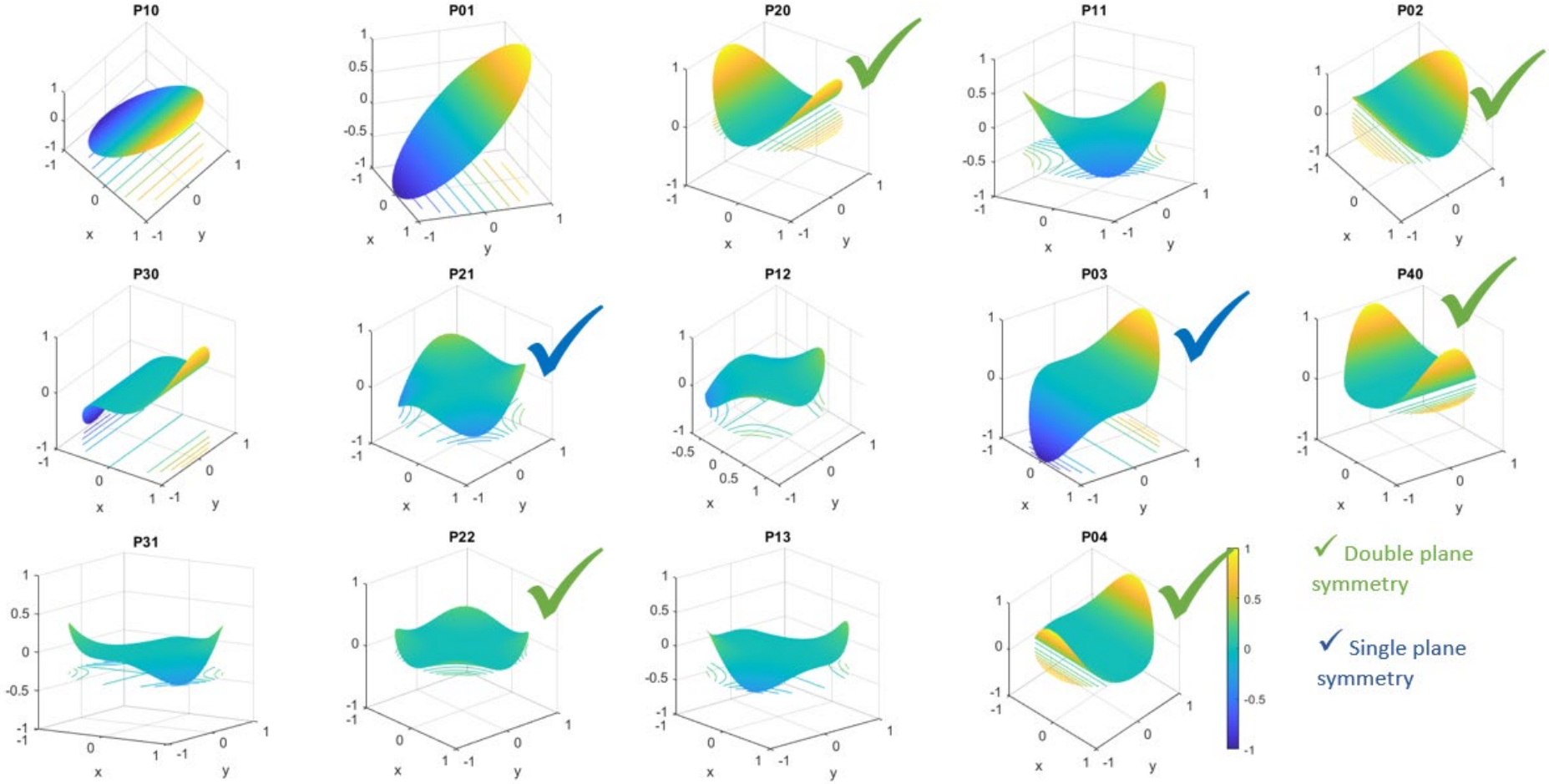

Figure 29 15 first elements of the polynomial power expansion Pmn

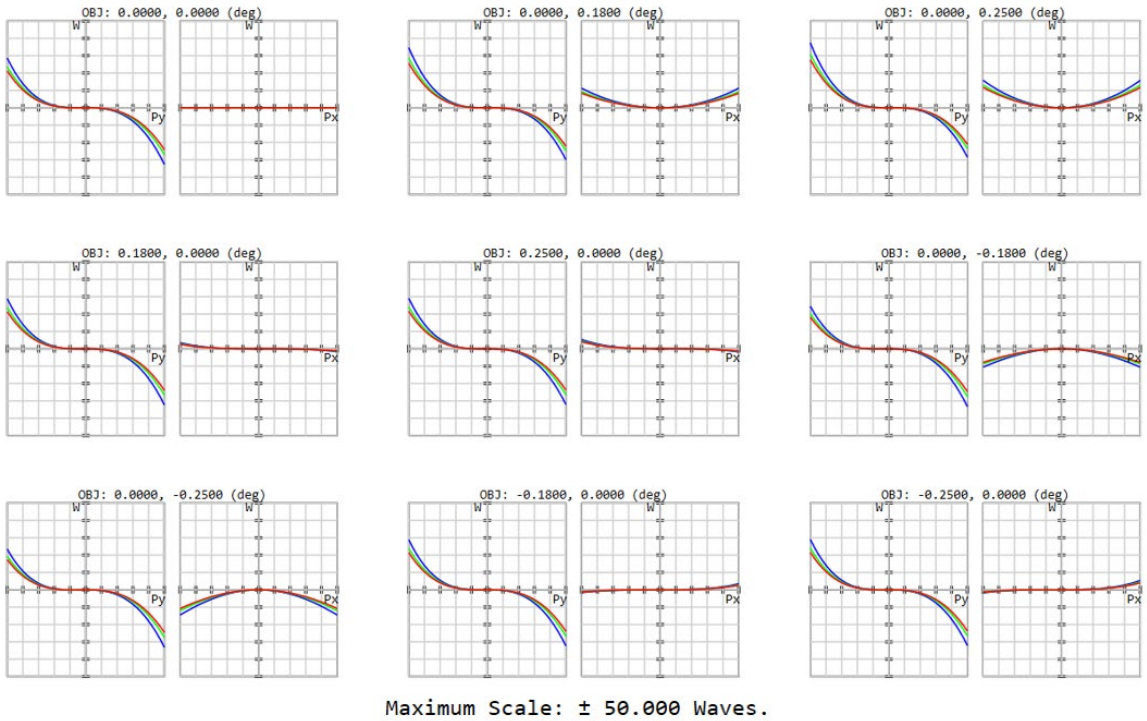

Figure 30 Wavefront aberration after implementation of extended polynomial surfaces.

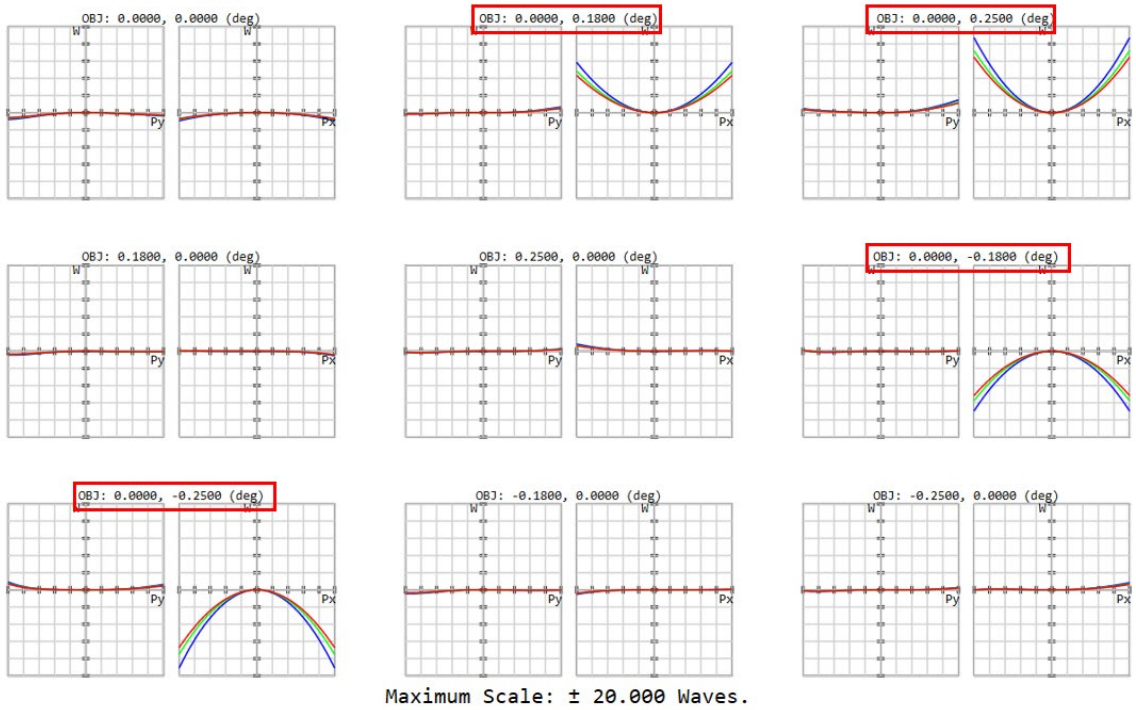

Figure 31 Wavefront aberration extended polynomial surfaces (P03 and P21) .

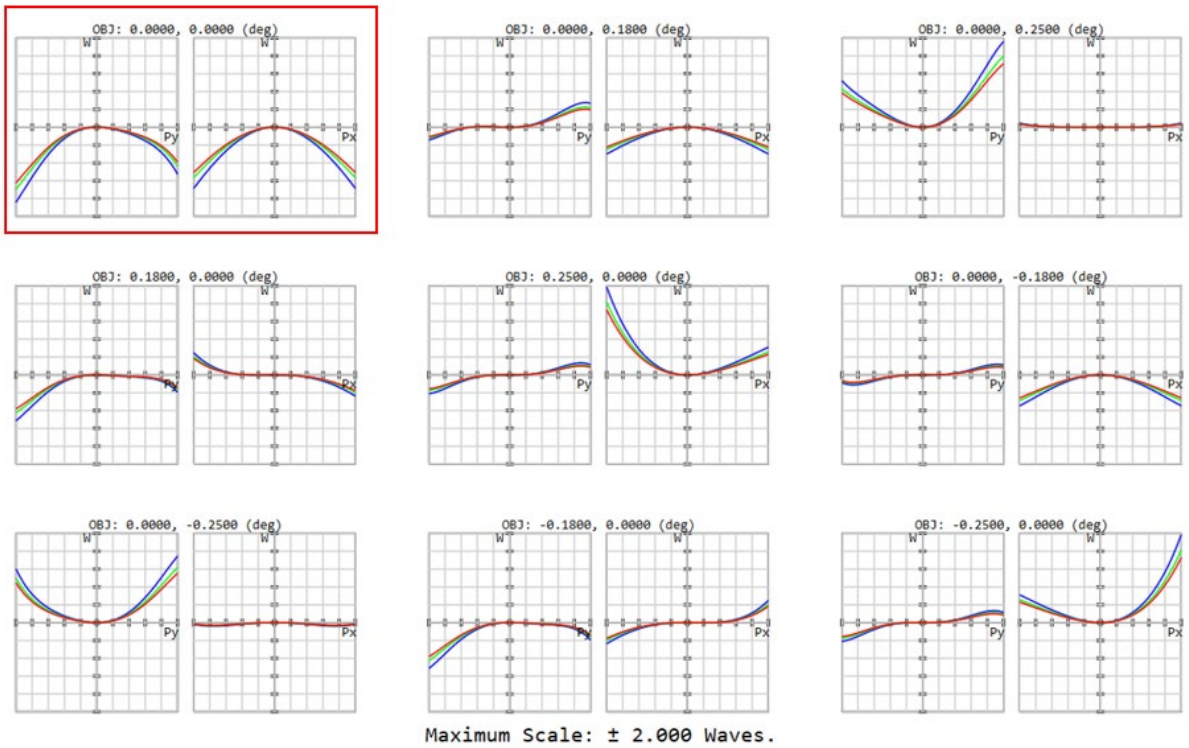

Figure 32 Wavefront aberration extended polynomial surfaces (P03, P21 and P20) .

	Surface Type	Comment	Thickness	Radius	Semi-Diameter	Conic	Par 3(unused)	X2Y0	X2Y1	X0Y3
0	OBJECT Standard		Infinity	Infinity	Infinity	0.000				
1	Standard		5000.000	Infinity	626.750	0.000				
2	Coordinate Break		0.000		0.000		6.000			
3	STOP (aper) Extended Polynomial	Primary	0.000	-11404.340 V	600.000 U	-1.093 V		-1.332E-07 V	-4.049E-10 V	-4.016E-10 V
4	Coordinate Break		-4000.000		0.000		6.000 P			
5	Coordinate Break		0.000		0.000		-10.078 V			
6	Extended Polynomial	Secondary	0.000	-5636.179 V	203.360	-6.933 V		1.205E-06 V	-6.348E-09 V	-6.356E-09 V
7	Coordinate Break		4200.000		0.000		-10.078 P			
8	IMAGE Standard		-	Infinity	62.290	0.000				

Figure 33 Complete prescription data for a TCT using extended polynomial surfaces

The MTF curves including the diffraction limited performance (black lines) are shown in Figure 34. Figure 35 shows spot diagram after optimization. A careful inspection of Figure 32 to Figure 35 reveals that the best performance of the system is not at center of the field of view as it is desirable for an optical telescope. The wavefront aberration fan for the central field (red rectangle) in Figure 32 shows that dominant aberration is defocus (parabolic profile in both pupil axes). In the MTFs curves (Figure 34) the central field point has almost the worst performance (red boxes) meanwhile points at the edge of the field are almost diffraction limited, this performance is also confirmed by the spot diagram (Figure 35) where the difference between the Ariry disc (black circle) is maximum in the central field point (red box). A possible explanation for this behavior is the introduction of defocus in the system to balance field curvature. There are some ways to improve the performance in central point: First, changing the weight of central field point via the "Field Data Editor", second, implementing a field flattener element such as a field lens or a thick meniscus lens. All these options were implemented, and the results obtained are analyzed in the next paragraphs.

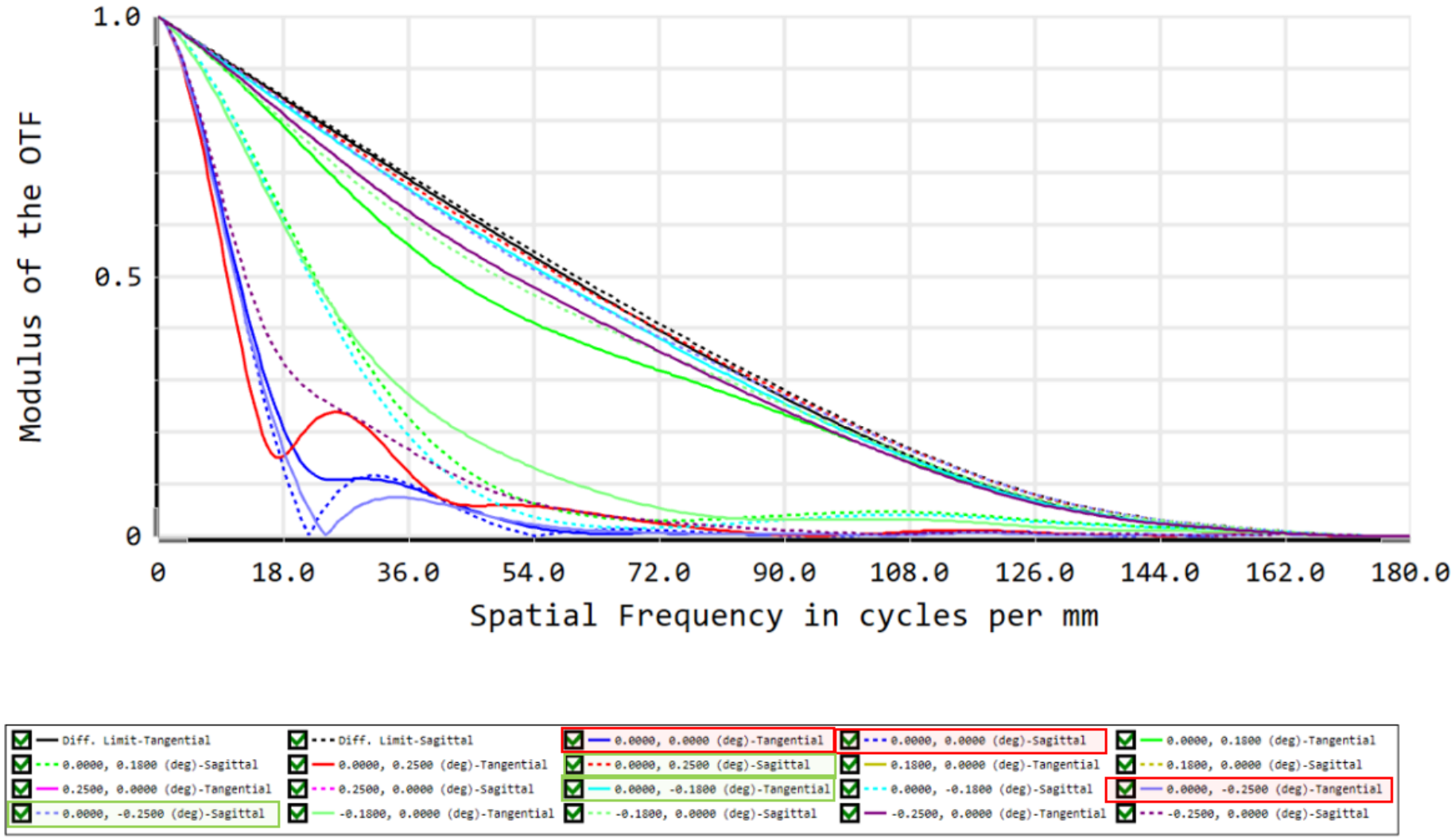

Figure 34 MTF for TCT system after optimization using conic constants and extended polynomial surface

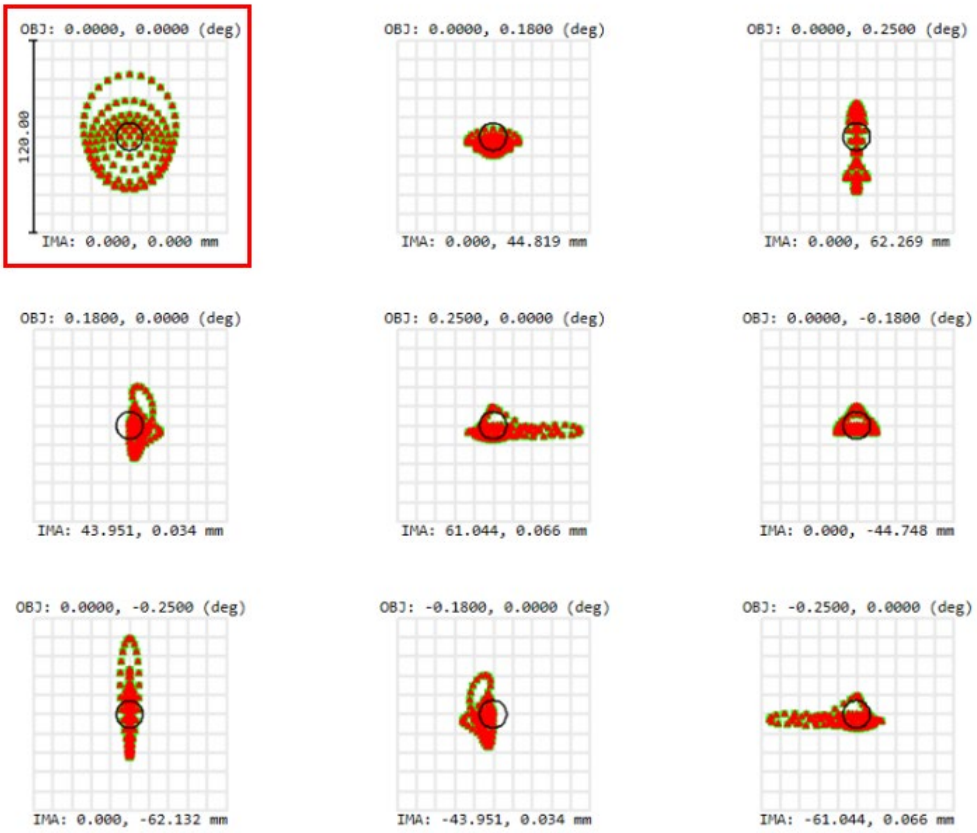

Figure 35 Spot diagram for a TCT system after optimization using conic constants and extended polynomial surface

Figure 36 shows a field data editor where 3 different weights were implemented: 100 for the central point, 3 for the intermediate points and 1 for the edge points. The wavefront aberration fans, the MTF curves and the spot diagram, after changing the weights of the view points and running a wavefront based optimization, are shown in Figure 37, Figure 38 and Figure 39. The three diagrams show an almost diffraction limited performance for the central field of view and a gradual degradation of the quality image from the center to the edge of the field. Figure 37 also confirms the presence of field curvature in the system. There is a parabolic profile proportional with the square of the field of view (always with the same sign) interacting with some high order aberrations.

	Comment	X Angle (°)	Y Angle (°)	Weight
1	Central point	0.000	0.000	100.000
2	Intermidiate Y+	0.000	0.180	3.000
3	Edge Y+	0.000	0.250	1.000
4	Intermediate X+	0.180	0.000	3.000
5	Edge X+	0.250	0.000	1.000
6	Intermediate Y-	0.000	-0.180	3.000
7	Edge Y-	0.000	-0.250	1.000
8	Intermediate X-	-0.180	0.000	3.000
9	Edge X-	-0.250	0.000	1.000

Figure 36 Field data editor with 3 different weights along the field of view.

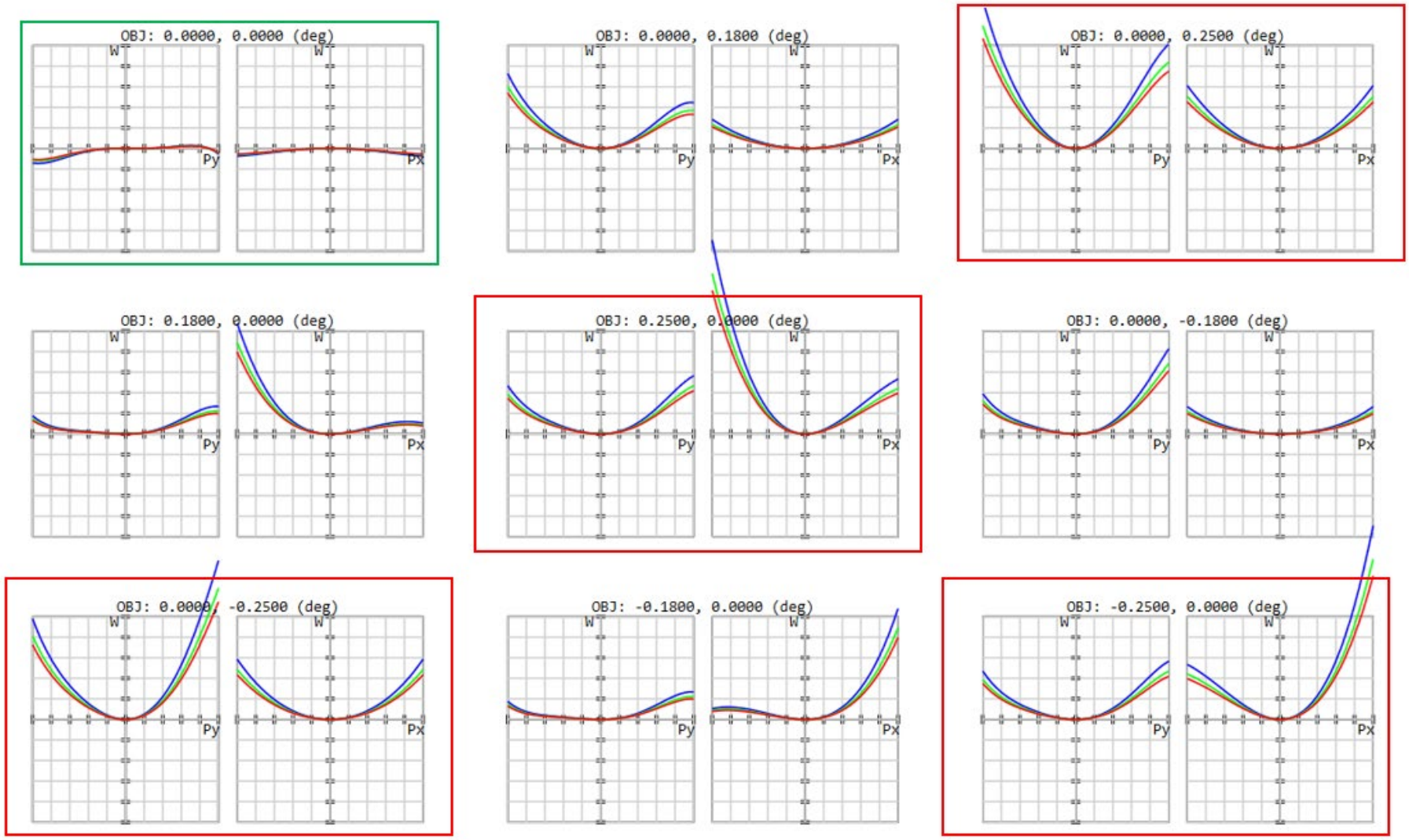

Figure 37 Wavefront aberration after changing the weight of the field points

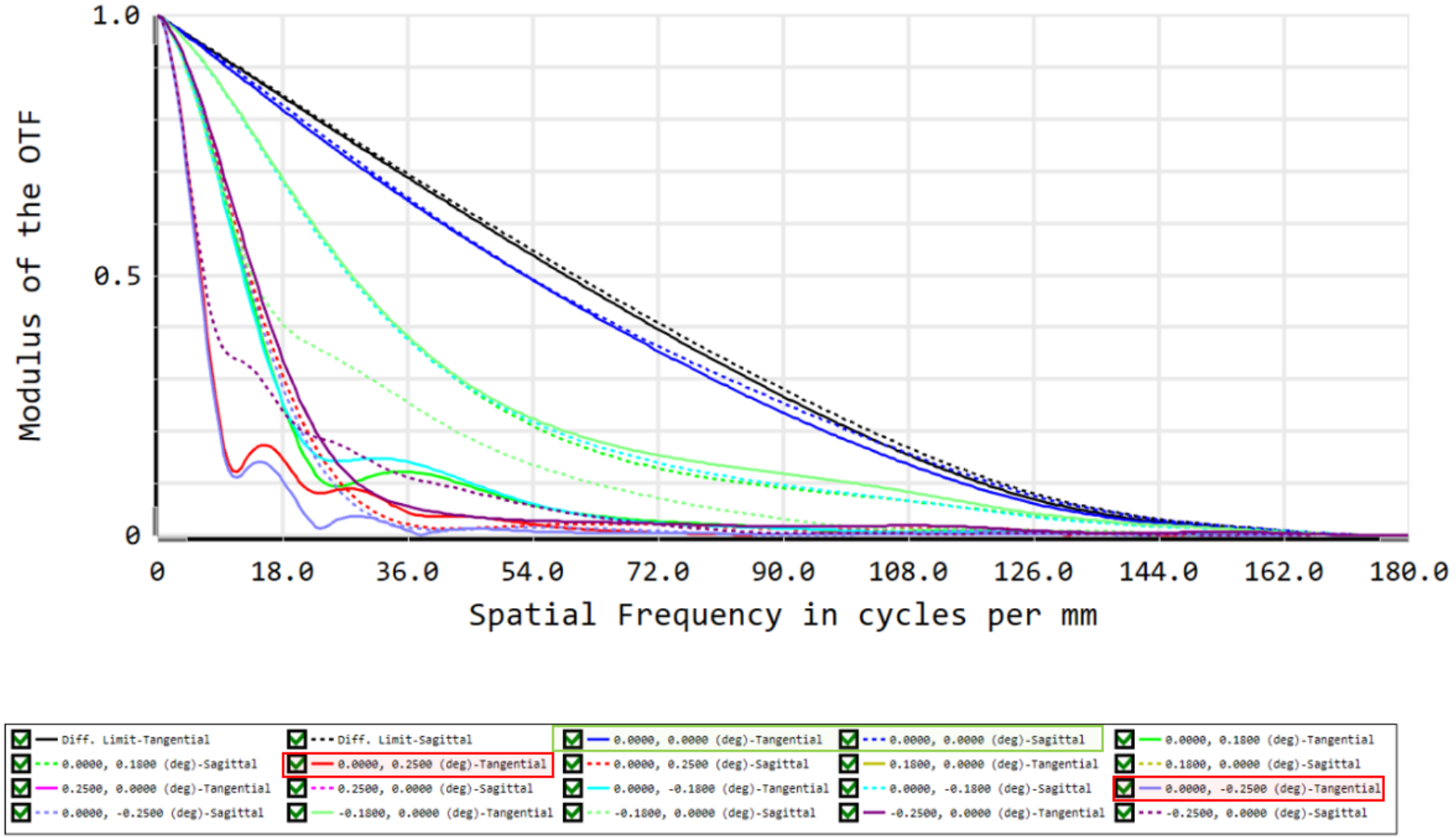

Figure 38 MTFs curves after changing the weight of the field points

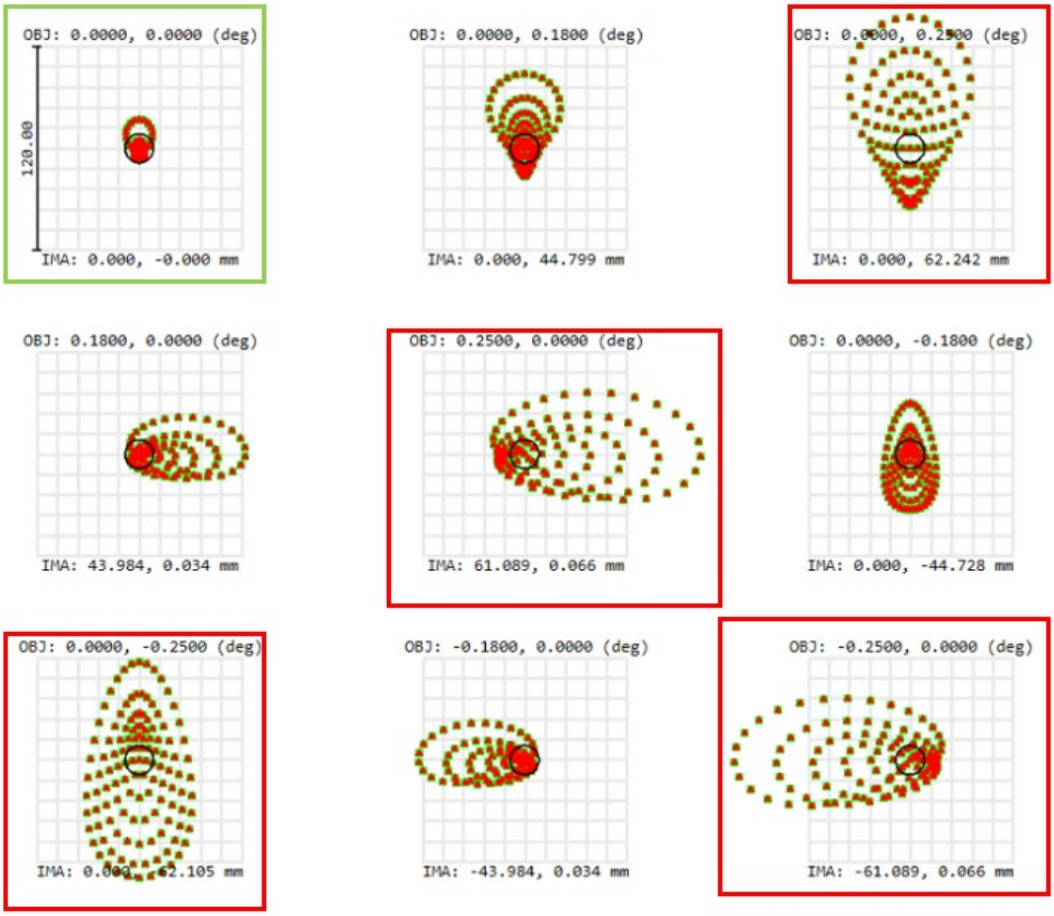

Figure 39 Spot diagrams after changing the weight of the field points

As an academic exercise two different field flatteners were implemented in the system described in Figure 33. They are shown in Figure 40. Option *a)* is based on a field lens just in front of the image plane, option *b)* uses as correction element a thick meniscus lens in the vicinity of the image plane. Both lenses were implemented in N-BK7 and with an aspect ratio diameter central thickness around 10:1.

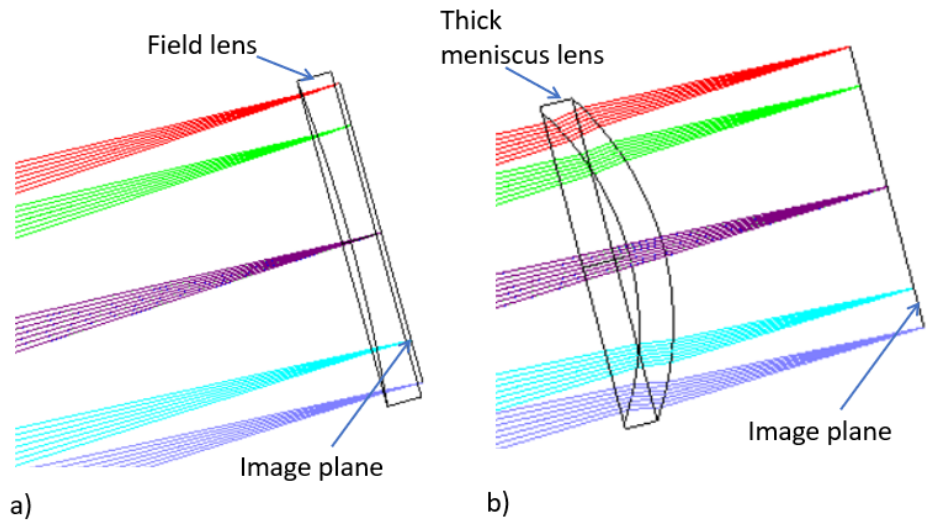

Figure 40 Two different option for field curvature correction a) Field lens, b) Thick meniscus lens

The results obtained for both designs are presented in Figure 41 (wavefront aberration fans) and Figure 42 (MTF curves). Figure 41 shows that the wavefront aberration is about 4 times lower in the thick lens solution with respect to the field lens. That means better performance for the second corrector solution, primarily in the zone highlighted by the red ellipse in Figure 42.

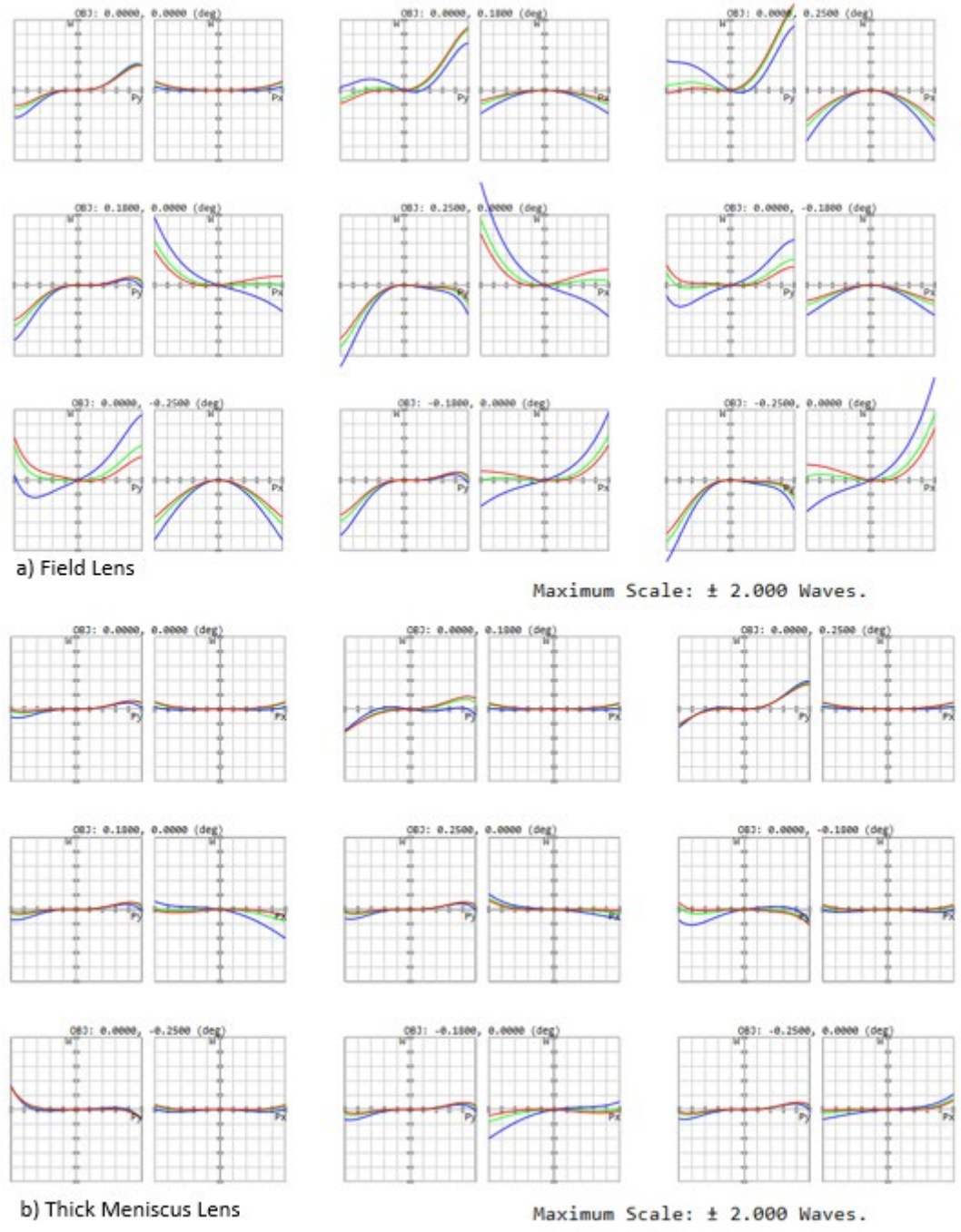

Figure 41 Wavefront aberration fans for two different field curvature correctors

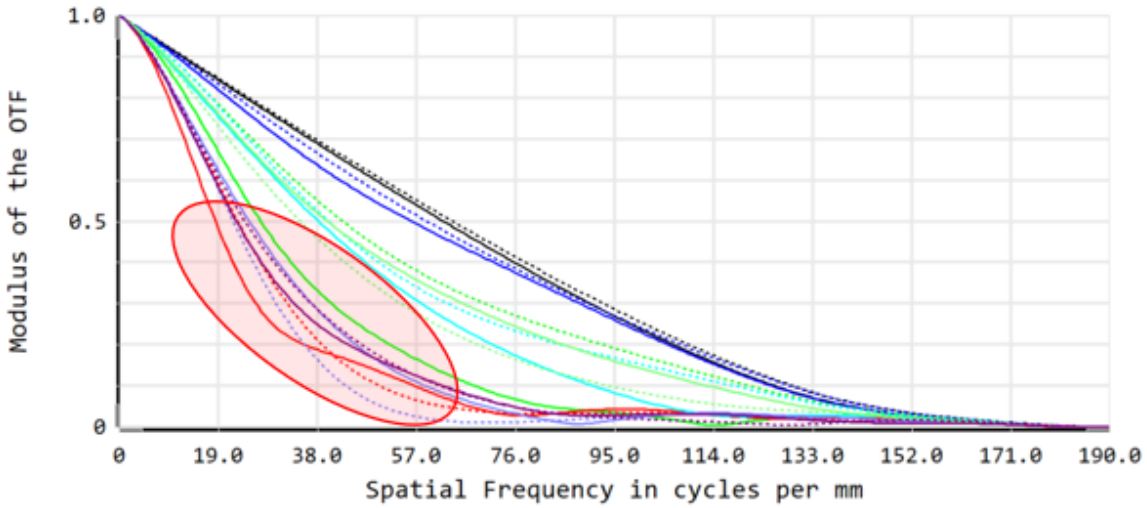

a) Field Lens

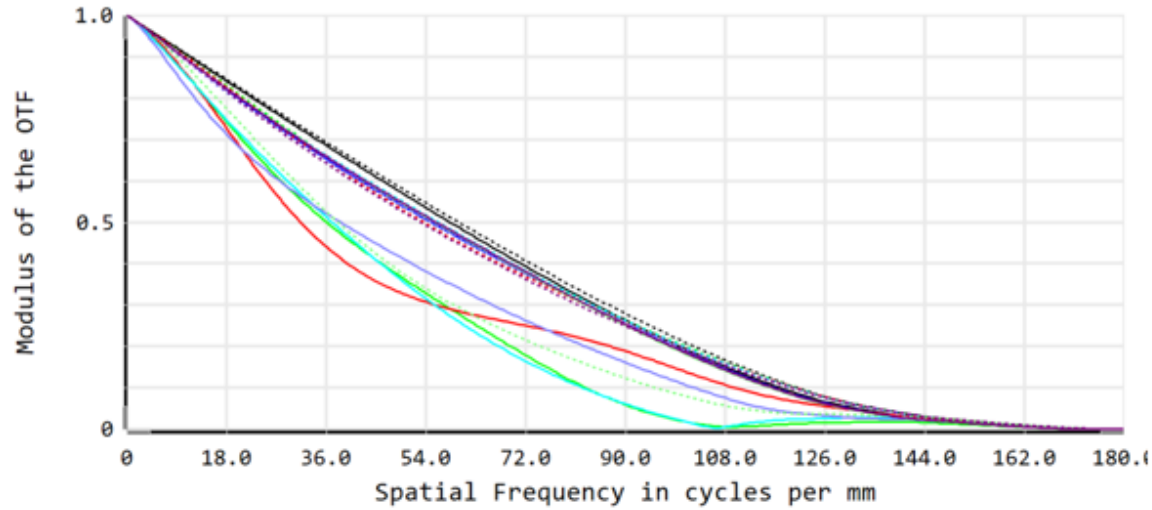

b) Thick Meniscus Lens

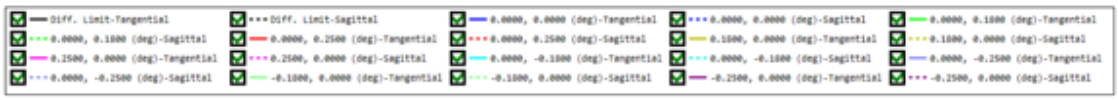

Figure 42 MTFs curves for two different field curvature correctors

6 Conclusion

- Simulation software is a very powerful vehicle, but the design of well corrected systems is still a work of engineering. In depth understanding of the interaction of the different elements is the path. It is there, in the understanding of relative basic concepts, such as third order aberrations, where a robust design with potential for optimization starts.

- Freeform surfaces are becoming more common due to the development of manufacturing processes, from plastic mold till electron beam figuring, passing through numerical control polishing and diamond turning of aspheric surfaces. These advances make the manufacturing of geometries that 50 years ago were only exercises in the drafting table possible. The possibilities are infinite in volume production, for example cell phones, but also in the most demanding applications such as astronomical instrumentation and semiconductor applications.

- This report is the final point of this master. It was an amazing journey. Not always easy, with its ups and downs, but writing this report I realize how much I have gained.

7 Bibliography

[1] J. Sasián, Introduction To Aberrations in Optial Imaging Systems, Cambridge: Cambridge University Press, 2013.

[2] J. Sasián, "How to approach the design of a bilateral symmetric optical system," *Optical Engineering,* vol. 33(6), 1994.

[3] J. W. Goodman, Introduction to Fourier Optics, New York: W. H. Freeman, 2017.

[4] T. Milster, Chapter 5: Scalar Diffraction [Lecture notes], Tucson, Arizona: Wyant College of Optical Science, University of Arizona, 2018.

[5] E. Hecht, Optics, Essex, England: Pearson, 2017.

[6] R. Liang, Opti 503 Lectures Material, Tucson Arizona: University of Arizona, 2021.

[7] J. Sasián, Introduction to Lens Design, Cambridge: Cambridge University Press, 2019.

[8] J. Sasian, "Method of Confocal Mirror Design," *Optical Engineering,* no. 58, 2019.